Archaeol Anthropol Sci
DOI 10.1007/s12520-016-0385-1

ORIGINAL PAPER

The ancient pozzolanic mortars and concretes of *Heliocaminus* baths in Hadrian's Villa (Tivoli, Italy)

Stefano Columbu [1] · **Fabio Sitzia** [1] · **Guido Ennas** [2]

Received: 30 May 2016 / Accepted: 6 September 2016
© Springer-Verlag Berlin Heidelberg 2016

Abstract The aim of this work is the physical and mineralogical-petrographic characterization of the mortars from the Baths with *Heliocaminus*, a special and unique architectural building in the complex of the Hadrian's Villa in Tivoli. Thirty samples were investigated for composition and physical properties (density, porosity, water absorption, mechanical strength, particle size distribution of aggregate, etc.), representative of eight mortar groups: *cubilia* bedding mortar, brick bedding mortars, floor-coating and wall-coating bedding mortars, floor (*rudus*) and wall conglomerates (*trullisatio*), vault concretes, and lime plasters (*arriccio*). Physical parameters, together with the microscopic analysis and binder/aggregate ratio determined in three ways using image analysis (on thin sections and on specimens) and weight-data from dissolution of binder, have shown an interesting relationship between the physical-compositional characteristics and the function of mortars within the structure of the *Heliocaminus* baths. To identify the minerals and the reactant phases between binder and aggregate, as well as the hydraulic degree, selected samples were analyzed with x-ray powder diffraction, thermogravimetry, and differential scanning calorimetry techniques. The obtained results provide a close relation between pozzolanic characteristics and physical-mechanical properties of the mortars (i.e., punching strength index).

Keywords Hadrian's Villa · Binder · Aggregate · TGA-DSC thermal analysis · XRPD analysis · Pozzolanic · Ancient mortars

✉ Stefano Columbu
columbus@unica.it

Guido Ennas
ennas@unica.it

[1] Department of Chemical and Geological Sciences, University of Cagliari, Via Trentino 51, 09127 Cagliari, Italy

[2] Department of Chemical and Geological Sciences, University of Cagliari—Cittadella Universitaria di Monserrato, 09042 Monserrato, Italy

Introduction

The personal baths of the Emperor Hadrian were built within the area of its Republican residence since 118 AD (Figs. 1 and 2). The baths were characterized by an imposing circular room, called *Heliocaminus*, warmed by sunlight and a traditional system with hypocaust (Mac Donald and Pinto 2006). This room has been recognized as a *sudatio* because of the presence of bakery openings that could supplement the heat derived from the floor and the wall necessary for the sauna (Salza Prina Ricotti 2000). The hall, covered by a coffered dome with central eye, was equipped with large windows, now fully collapsed, facing the south-western side, where all the Hadrian Villa heated rooms were located. This orientation reflects faithfully the requirements dictated by architect *Vitruvio* (Cicerchia 1985; Giuliani Cairoli 2006; Pollione 15 BC; Verduchi 1975). The building with *Heliocaminus* presents innovative architectural features that were given by the same Emperor Hadrian (Mac Donald and Pinto 2006).

The construction materials such as marble coating, already studied by several authors with various methods (Antonelli et al. 2013; Attanasio et al. 2009, 2013; Columbu et al. 2014a; Lapuente et al. 2012; Pensabene et al. 2012), the stone filling of the curtain walls, and the not decorated mosaic in the corridors of floors are rather similar to those used in other

Published online: 27 September 2016

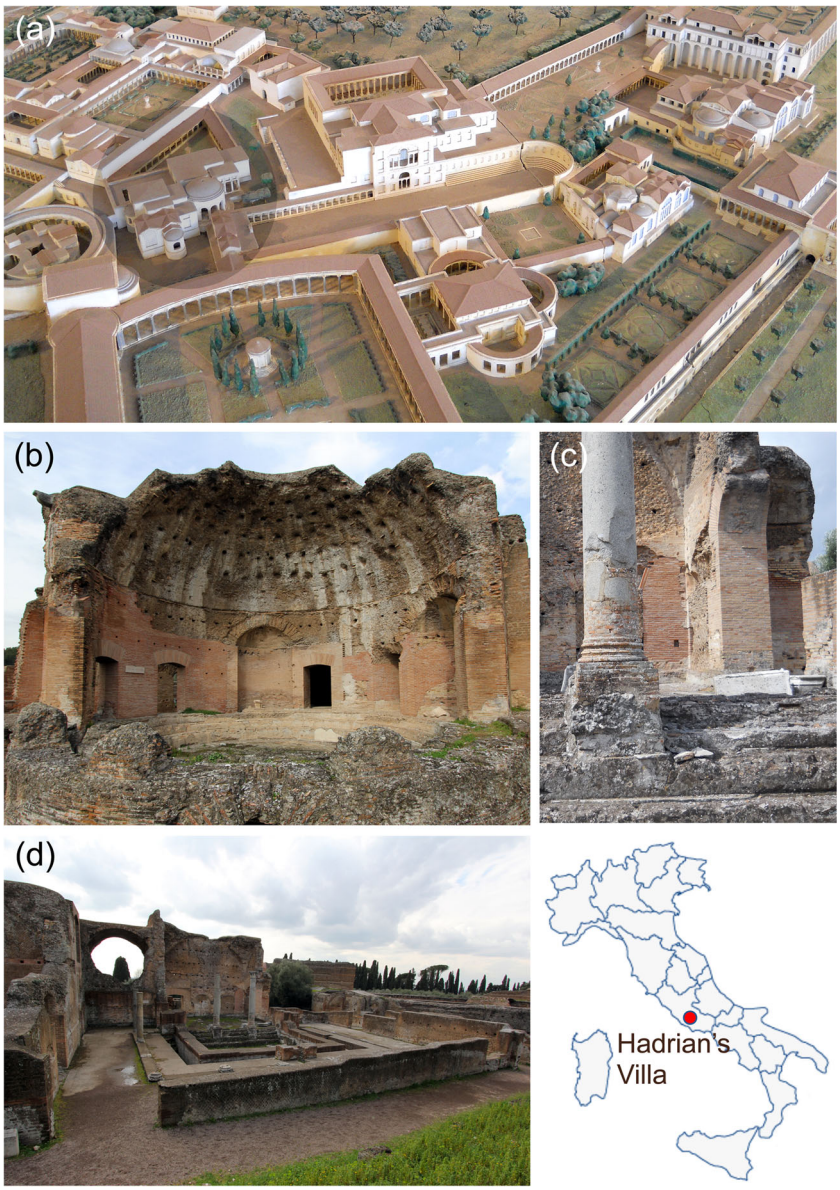

Fig. 1 **a** Photo-overview of 3D model of Hadrian's Villa (made by Italo Gismondi in 1956), where it highlights the *Heliocaminus* bath (on the *central left*); **b** view of *Heliocaminus* room; **c**, **d** *Natatio* room

buildings of the Villa and confirms the relevance of the complex to the noble zone (Adam 2006; Cagnana 2000).

In many buildings of Hadrian's Villa, volcanic rocks (i.e., pyroclastites) outcropping in the same area of the residence were frequently used. The pyroclastic rocks have been frequently used in historical times in both mortars and as a building material in the masonry or as tool (e.g., Antonelli et al. 2014; Bertorino et al. 2002; Coroneo and Columbu 2010; Columbu et al. 2011, 2013, 2014c, 2015c; Columbu and Guccini 2013; Macciotta et al. 2001; Melis and Columbu 2000). In the *Heliocaminus* Baths, these materials are primarily used as construction element in the walls (i.e., *cubilia*), and considered their mainly matrix glass, even as pozzolanic aggregate.

For laying all several kinds of construction materials, different types of aerial and hydraulic mortars were used in Hadrian's Villa for bedding bricks, stone ashlars, marble slabs, and plaster (Fig. 2).

The mortars show a variable composition and hydraulic degree according to their function in building, e.g., to improve the physical-mechanical strength (i.e., wall structure, foundations, raised floors, etc.) or as waterproofing (i.e., cisterns).

The hydraulic mortars were especially used in moist environments such as Roman spa. In these cases (e.g., *Heliocaminus* Baths), the pozzolanicity is generally conferred by *cocciopesto* or glassy volcanic aggregates (e.g., scoria).

The compositional characteristics of the mortars are fundamental to define the construction phases of ancient buildings and to trace the technologies used in the historical periods (Columbu et al. 2015b; Crisci et al. 2001, 2002; De Luca et al. 2013; Maravelaki-Kalaitzaki et al. 2003; Miriello et al. 2010a, b, 2015; Moropoulou et al. 1995, 1999, 2000, 2002,

Fig. 2 *Heliocaminus* Baths: **a** mortar of brick wall; **b** wall of Natatio masonry room with *cubilia* bedding mortar; **c** internal view with mortars of floor (down) and wall (in front) coating for slab marble; **d** detail of sample ADTH 7 (wall coating mortar); **e** floor conglomerates with *cocciopesto* (suspensura); **f** wall coating and conglomerates with *cocciopesto* of *Frigidarium* room; **g** vault concretes of collapsed vault; **h** wall with plaster (sample ADTH 14)

2003a, b, 2004, 2005; Paama et al. 1998; Palomo et al. 2002; Riccardi et al. 1998; Smith and Smith 2009; Vola et al. 2011), especially when in combination with 3D laser-scan relief methods of the monument structures (Columbu and Verdiani 2011, 2012, 2014; Lezzerini et al. 2016; Verdiani and Columbu 2010, 2012).

Also, the physical properties (porosity, bulk density, mechanical strength, etc.) are significant for the basic characterization of geomaterials (Columbu et al. 2015a), to study the alteration processes (Columbu et al. 2014b), and consequently to address the conservation and restoration interventions (Callebaut et al. 2001; Moropoulou et al. 2013).

The following paper is a work started by Columbu et al. (2015b). It proposes the study of the bedding mortars, conglomerates, and concretes from *Heliocaminus* Baths through an archaeometric multidisciplinary approach characterized by mineralogical–petrographic–physical–mechanical analysis, including particle size of the aggregate. Thirty mortar samples from main sectors of the theater (i.e., *tribunalia* vaults, *cavea* tiers, stage walls, vaults, brick walls of external niches, structure masonry) were analyzed. The analysis are addressed to define the mixture technologies of raw material according to ancient Roman mode and uses (Adriano et al. 2009; Bultrini et al. 2006; Miriello et al. 2010, 2011; Stanislao et al. 2011).

By polarizing microscope analysis, the mineralogical composition and petrographic characteristics of mortars were determined. The petrographic study, together with image analysis on thin sections and on bulk mortar specimen faces, can provide significant data about (1) preparation of mortars and different mixing ratios of binder and aggregate, (2) geological origin of raw materials used as aggregate (e.g., volcanic scoria, leucitites), and (3) selection method of raw materials in relation to the function of mortar in the building.

To define the hydraulic degree of mortars, on enriched binder powdered samples, thermogravimetric and differential scanning calorimetry (TG and DSC) and XRD analysis were made, according to well-known experimental methods (Babini and Fiori 1996; Bakolas et al. 1998; Bultrini et al. 2006; Drdácky et al. 2013; Maravelaki-Kalaitzaki et al. 2003; Miriello et al. 2010, 2011; Moropoulou et al. 1995, 1999, 2003a, b; Ricciardi et al. 1998; Ortega et al. 2008; Palomo et al. 2011; Topçu and Isıkdag 2013). Analytical data were compared to the physical-mechanical properties (i.e., point load strength index) to define their relationship (Papayianni et al. 2013; Topçu and Isıkdag 2013).

Furthermore, the analysis of other physical properties (water absorption and saturation) allows us to verify the production quality of mortars.

Materials and methods

Materials

Thirty samples of mortars collected from the *Heliocaminus* Baths were analyzed (Fig. 3). The samples are representative of mortars with different functions in the baths (according to eight groups, Columbu et al. 2015b; Table 1), such as (see Fig. 3 and its caption) seven brick bedding mortars (*Opus Testaceum*), three *Cubilia* bedding mortars (*Opus Reticolatum*), four floor-coating bedding mortars (*Marmor pavimentum*), three wall-coating bedding mortars (*Harenata marmor*), five floor

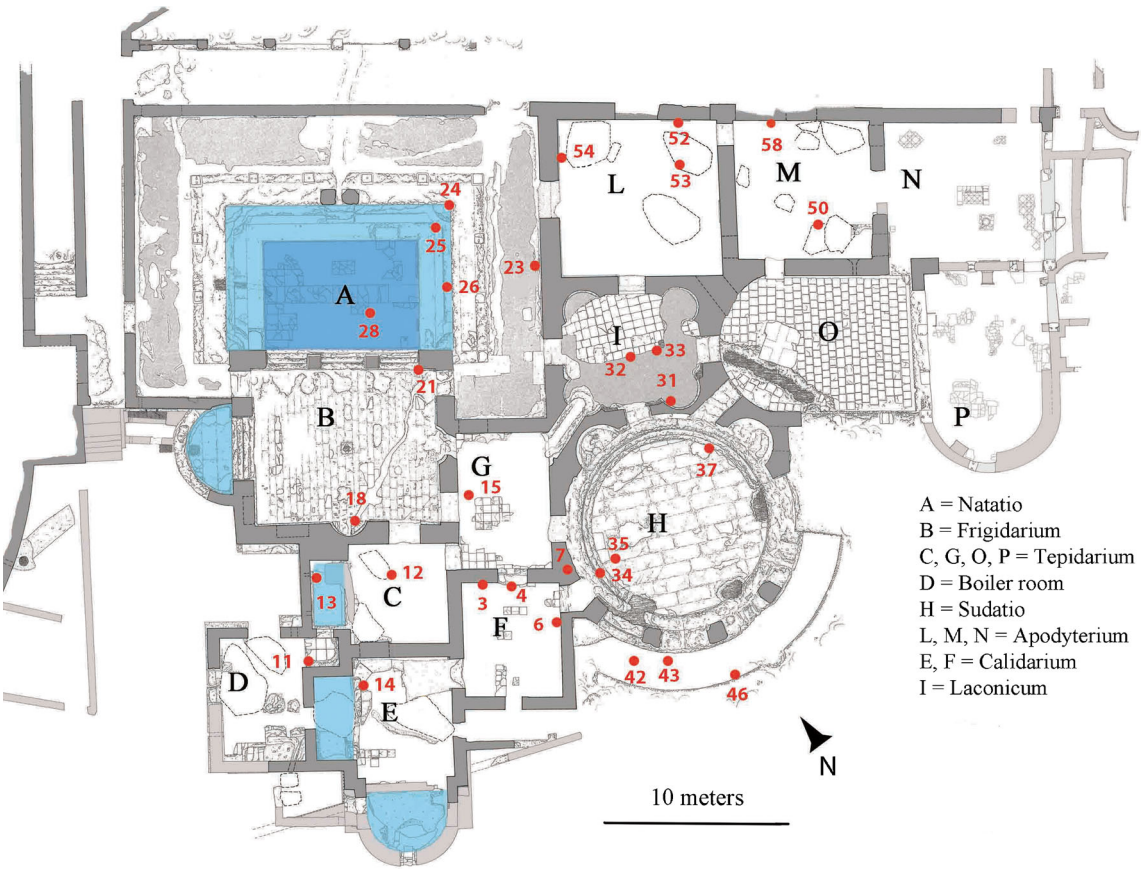

Fig. 3 Map of *Heliocaminus* Baths with sampling points of mortars. Sample codes referring to mortar groups (according to Table 1): seven brick bedding mortars = ADTH 4, 6, 11 (fire room), 21, 35, 42, 43; three *Cubilia* bedding mortars = sample ADTH 23, 46, 54; four floor-coating bedding mortars = ADTH 24, 28, 34, 37; three wall-coating bedding mortars = ADTH 7, 31, 52; five floor-conglomerates = ADTH 3, 15, 25, 32, 33; three wall-conglomerates = ADTH 18, 26, 58; three vault concretes = ADTH 12, 50, 53; two plasters (*arriccio* layers) = ADTH 13, 14

Table 1 Compositional characteristics by microscopic analysis of the mortars from the *Heliocaminus* Baths, where localization, sampling height, and percentage distribution of different aggregates are reported

Mortar typology	Sample	Room of baths	Height (cm)	Fragments (%)				Crystal-clasts (%)		
				Scoria	Leucitite	*Cocciopesto*	Marble	Cpx	Hnb	Bt
Brick bedding mortars	ADTH 4	*Calidarium*	−98	99.5	0	0	0.5	0	0	0
	ADTH 6	*Calidarium*	−35	99.1	0.7	0	0.2	0	0	0
	ADTH 11	*Fire room*	−85	98.2	1.5	0	0	0.3	0	0
	ADTH 21	*Natatio*	90	99.8	0	0	0.2	0	0	0
	ADTH 35	*Sudatio*	−16	94.3	3.8	0	0	1.9	0	0
	ADTH 42	*Sudatio*	−98	96.8	1.1	0	0.1	0.9	1.1	0
	ADTH 43	*Sudatio*	7	99.4	0	0	0.6	0	0	0
Cubilia bedding mortars	ADTH 23	*Natatio*	58	99.9	0	0	0.1	0	0	0
	ADTH 46	*Sudatio*	−23	97.8	0.8	0	0.2	1.2	0	0
	ADTH 54	*Apodyterium*	107	95.7	2.1	0	0.3	1.2	0.7	0
Floor-coating bedding mortars	ADTH 24	*Natatio*	−25	95.4	0	4.3	0	0	0.3	0
	ADTH 28	*Natatio*	−138	87.9	1.0	5.1	0	1.0	4.0	1.0
	ADTH 34	*Sudatio*	−4	95.2	0	4.8	0	0	0	0
	ADTH 37	*Laconicum*	−64	95.1	0	4.5	0	0.4	0	0
Wall-coating mortars	ADTH 7	*Calidarium*	28	98.0	0	0	0	1.0	1.0	0
	ADTH 31	*Laconicum*	25	98.3	0.8	0	0	0	0.9	0
	ADTH 52	*Apodyterium*	20	99.3	0	0	0	0.7	0	0
Floor conglomerates (*rudus*)	ADTH 3	*Calidarium*	−10	85.7	0	13.8	0	0.5	0	0
	ADTH 15	*Tepidarium*	−12	87.9	0	12.1	0	0	0	0
	ADTH 25	*Natatio*	−28	79.8	3.2	15.2	0	1.8	0	0
	ADTH 32	*Laconicum*	−7	78.7	5.1	16.2	0	0	0	0
	ADTH 33	*Laconicum*	−5	81.0	2.1	15.3	0	0	1.6	0
Wall conglomerates (*trullisatio*)	ADTH 18	*Frigidarium*	30	73.1	7.7	17.7	0	0.9	0.6	0
	ADTH 26	*Natatio*	−109	76.5	2.7	20.4	0	0	0.4	0
	ADTH 58	*Apodyterium*	26	85.1	1.1	13.8	0	0	0	0
Vault concretes	ADTH 12	*Calidarium*	0	98.5	0.9	0	0.1	0	0.5	0
	ADTH 50	*Apodyterium*	52	98.7	0	0	0.1	1.2	0	0
	ADTH 53	*Apodyterium*	58	99.8	0	0	0.2	0	0	0
Plasters	ADTH 13	*Tepidarium*	−7	84.4	5.2	8.2	0	0	2.2	0
	ADTH 14	*Calidarium*	40	81.7	0	16.6	0	1.4	0.3	0

conglomerates (*Opus Signinum* of *Rudus*), three wall conglomerates (*Opus Signinum* of *Trussillatio* or *rinzaffo* layers), three concretes of collapsed vaults (*Opus Caementitium*), and two plasters (*arriccio* layers).

Four lime lumps of mortars were also analyzed to understand their composition and modality of formation. The mortars with the same function were sampled according to different heights in the structure and/or in diverse environments.

Samples of mortar and stone were taken from the superficial portions of monument material, with a maximum volume of about 25 cm^3, compatibly with the limits imposed by the Superintendence of Cultural Heritage of Lazio Region. However, the size of the material taken from the baths is representative and suitable to determine the compositional and physical characteristics of the studied mortars.

Analytical methods

Petrographic determinations of mineralogical composition were carried out by optical polarized microscopy on polished thin sections on 38 samples of which 30 mortars consolidated by epoxy resin, 3 *lateritious*, and 5 volcanics. Modal analysis of mortars has been determined with "points counter" on about 300 points for each thin section.

The binder/aggregate ratio (B/A) of mortars was calculated through image analysis (by ImageJ 1.47v) in two different ways: (1) on photographs taken on six faces of the cubic specimens of mortars on which the physical-mechanical tests have been determined and (2) on thin-section photographs detected with the flatbed scanner. The binder/aggregate ratio (B/A) was calculated also with weight data from acid

dissolution of mortar binder to determine the particle size of aggregate (see text and figure captions of manuscript).

A Seifert X3000 apparatus in the Bragg–Brentano geometry was used for x-ray powder diffraction. It was operated using the CuKα radiation in the range of 8–40 (2ϑ degrees) with step of 0.05 2ϑ, with an opportune counting time to optimize the signal/noise ratio. JCPDF-2 database was used for the identification of the phases.

Regarding the thermogravimetric analysis, 2 g of each mortar (without the coarse aggregate) were ground by Giuliani IG colloidal mill W2/E/S. To enrich the sample in the binder fraction, the powder was treated with Frantz magnetic separator for the removal of the iron-magnetic mineral fraction belonging mainly to the volcanic aggregate.

Thermogravimetric analysis (TGA) measurements were carried out at atmospheric pressure using a Perkin Elmer instrument model TGA7. The measurements were performed under Ar flow (60 mL/min). Samples of 10 mg were placed in platinum crucibles and scanned in the temperature range of 30–900 °C with a heating rate of 10 °C/min. TGA7 instrument was calibrated with Curie points of Alumel, Nickel, Perkalloy, and Iron standard samples, and the temperature was obtained with an accuracy of ±2 °C. Differential scanning calorimetry (DSC) measurements were carried out at atmospheric pressure using a Perkin Elmer instrument model DSC7. The measurements were performed under Ar flow (60 mL/min). Samples of 5 mg were placed in platinum crucibles and scanned in the temperature range of 30–650 °C with a heating rate of 10 °C/min. DSC7 instrument was calibrated by measuring the melting temperature of metallic indium and zinc (99.999 mass % purity) and the temperature was obtained with an accuracy of ±0.5 °C.

Physical tests were determined on 82 cubic specimens (with an average size of 15 × 15 × 15 mm) extracted from unaltered portion of samples after removing the exterior part of mortar. The physical properties analysis was made also on a small

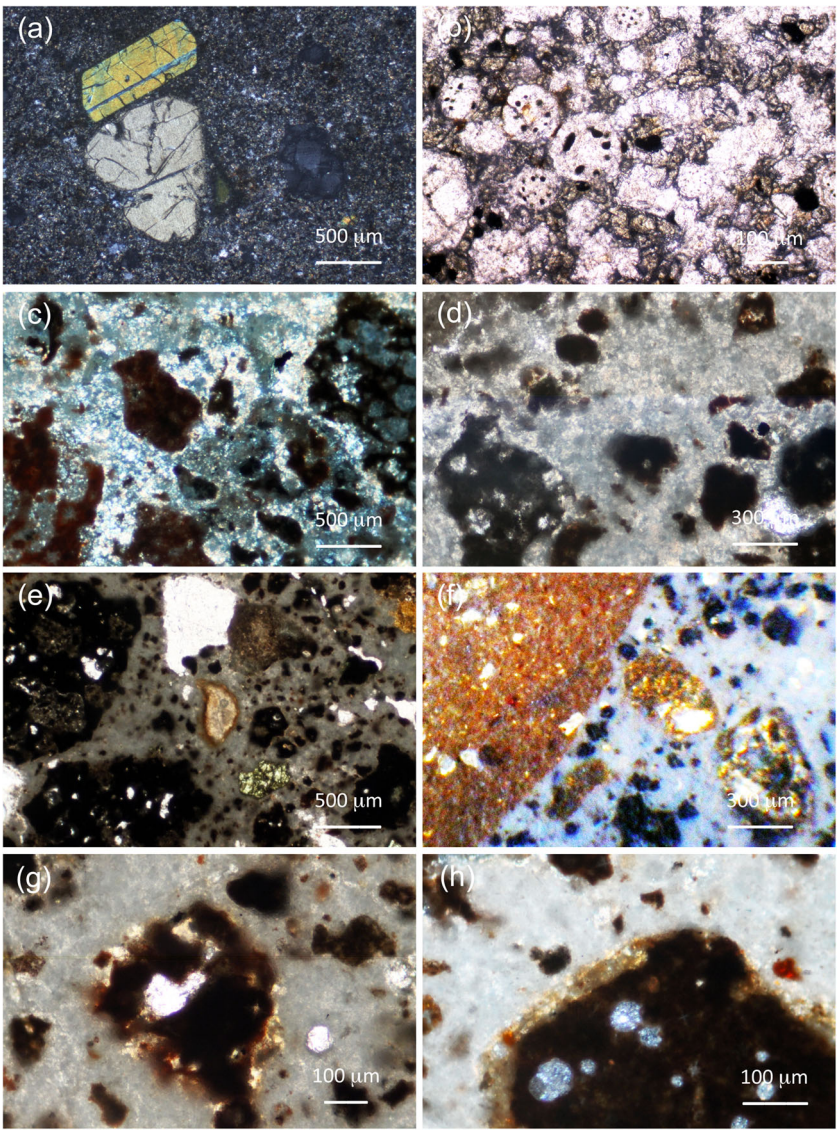

Fig. 4 Micro-photographs on thin section of mortars and aggregates: **a** cross Nicol: phenocrysts immersed in microcrystalline groundmass in leucitic basalt; **b** plain polars: leucite crystals in leucitites; **c**, **d** plain polars: vesicular black and red scoria with binder reaction border; **e**, **f** plain polars: vesicular black scoria and *cocciopesto* fragments with reaction border with binder; **g**, **h** vesicular black scoria with obvious reaction border with binder (inside scoria fragment, there are two leucite crystals)

fragment (only for some mortar samples) of volcanic and aggregates extracted from mortars. Specimens were dried at 105 ± 5 °C and then the dry solid mass (m_D) was determined. The solid phases volume (V_S) of powdered rock specimens (on 5–8 g and with particle size less than 0.063 mm) and the real volume (with $V_R = V_S + V_C$, where V_C is the volume of pores closed to helium) of the specimens were determined by helium ultrapycnometer 1000 (Quantachrome Instruments).

Then, the wet solid mass (m_W) of the samples was determined after water absorption by immersion for 10 days. Through a hydrostatic analytical balance, the bulk volume V_B (with $V_B = V_S + V_O + V_C$, where $V_O = (V_B - V_R)$ is the volume of open pores to helium) is calculated as

$$V_B = [(m_W - m_{HY})/\rho_w T_{25°C}]\cdot 100$$

where m_{HY} is the hydrostatic mass of the wet specimen and $\rho_W T_{25°C}$ is the water density at a temperature of 25 °C.

Total porosity (Φ_T), open porosity to water and helium ($\Phi_O H_2O$ and $\Phi_O He$, respectively), closed porosity to water and helium ($\Phi_C H_2O$, $\Phi_C He$), bulk density (ρ_B), real density (ρ_R), and solid density (ρ_S) were computed as

$$\Phi_T = [(V_B - V_S)/V_B]\cdot 100$$
$$\Phi_O H_2O = \left[(m_W - m_D)/{}_W T_X\right]/V_B\cdot 100$$
$$\Phi_O He = [(V_B - V_R/V_B)]\cdot 100$$
$$\Phi_C H_2O = \Phi_T - \Phi_O H_2O$$
$$\Phi_C He = \Phi_T - \Phi_O He$$
$$\rho_S = m_D/V_S;\ \rho_R = m_D/V_R;\ \rho_B = m_D/V_B$$

Table 2 Circularity data of mortar aggregate of mortars determined by image analysis on thin section, where circularity variation ranges, averages, means of average circularity data, standard deviations, and variation coefficients are reported

Mortar typology	Sample	Circularity variation range (min–max)	Average circularity	Mean of average circularity	Standard deviation	Variation coefficient
Brick bedding mortars	ADTH 4	0.02–0.99	0.67	0.57	0.07	0.12
	ADTH 6	0.08–0.99	0.57			
	ADTH 11	0.04–1	0.50			
	ADTH 21	0.05–0.96	0.45			
	ADTH 35	0.01–0.99	0.59			
	ADTH 42	0.05–0.99	0.61			
	ADTH 43	0.06–0.98	0.58			
Cubilia bedding mortars	ADTH 23	0.03–1	0.54	0.59	0.05	0.09
	ADTH 46	0.04–1	0.58			
	ADTH 54	0.01–1	0.64			
Floor-coating bedding mortars	ADTH 24	0.04–0.98	0.53	0.54	0.04	0.07
	ADTH 28	0.05–1	0.48			
	ADTH 34	0.03–1	0.56			
	ADTH 37	0.01–1	0.58			
Wall-coating bedding mortars	ADTH 7	0.03–1	0.64	0.52	0.11	0.21
	ADTH 31	0.04–0.99	0.45			
	ADTH 52	0.01–0.99	0.46			
Floor cocciopesto conglomerates (*rudus*)	ADTH 3	0.03–0.99	0.58	0.54	0.04	0.07
	ADTH 15	0.03–0.99	0.50			
	ADTH 25	0.07–0.99	0.52			
	ADTH 32	0.02–1	0.52			
	ADTH 33	0.02–1	0.59			
Wall cocciopesto conglomerates (*trullisatio*)	ADTH 18	0.01–1	0.58	0.59	0.02	0.04
	ADTH 26	0.06–0.99	0.61			
	ADTH 58	0.01–0.97	0.57			
Vault concretes	ADTH 12	0.03–0.99	0.59	0.58	0.02	0.03
	ADTH 50	0.02–0.99	0.56			
	ADTH 53	0.04–1	0.59			
Plasters	ADTH 13	0.04–1	0.56	0.57	0.01	0.02
	ADTH 14	0.02–0.97	0.58			

The weight imbibition coefficient (IC_W) and the saturation index (SI) were computed as

$$IC_W = [(m_W - m_D)/m_D] \cdot 100$$
$$SI = (\Phi_O H_2O/\Phi_O He) = [(m_W - m_D)/\rho_W T_X]/V_O \cdot 100$$

The punching strength index was determined with a Point Load Tester (mod. D550 Controls Instrument) according to ISRM (1972, 1985) on the same pseudo-cubic rock specimens used for other physical properties. The force was exerted via the application

Table 3 Comparison data of binder/aggregate ratio of all mortars determined on three different methods: by image analysis on thin section, on cubic bulk mortar specimens, and using weight data from acid dissolution of binder

Mortar typology	Sample	By image analysis on cubic specimens (vol.%)			By image analysis on thin section (vol.%)			By binder dissolution (vol.%)			Vitruvio's recommended values	
		Aggregate	Binder	B/A	Aggregate	Binder	B/A	Aggregate	Binder	B/A	Aggregate vol.%	Mortar thickness
Brick bedding mortars	ADTH 4	63.31	36.69	0.58	63.15	36.85	0.58	76.64	23.36	0.30	65–70	1.5–2
	ADTH 6	65.37	34.63	0.53	55.04	44.96	0.82	76.15	23.85	0.31		
	ADTH 11	48.95	51.05	1.04	63.90	36.10	0.56	82.05	17.95	0.22		
	ADTH 21	59.08	40.92	0.69	60.68	39.32	0.65	78.82	21.18	0.27		
	ADTH 35	72.09	27.91	0.39	61.95	38.05	0.61	81.30	18.70	0.23		
	ADTH 42	50.95	49.06	0.96	40.19	59.81	1.49	80.06	19.94	0.25		
	ADTH 43	60.14	39.86	0.66	52.05	47.95	0.92	79.42	20.58	0.26		
	Means	59.98	40.02	0.69	56.71	43.29	0.80	79.21	20.79	0.26		
Cubilia bedding mortars	ADTH 23	67.04	32.96	0.49	48.87	51.13	1.05	74.66	25.34	0.34	65–70	1.5–2.5
	ADTH 46	57.77	42.23	0.73	48.35	51.65	1.07	77.50	22.50	0.29		
	ADTH 54	60.73	39.27	0.65	48.69	51.31	1.05	83.66	16.34	0.20		
	Means	61.85	38.15	0.62	48.64	51.36	1.06	78.61	21.39	0.28		
Floor-coating bedding mortars	ADTH 24	63.35	36.65	0.58	46.60	53.40	1.15	81.71	18.29	0.22	70–80	3.5–6
	ADTH 28	69.35	30.65	0.44	44.55	55.45	1.24	80.69	19.31	0.24		
	ADTH 34	65.04	34.96	0.54	35.61	64.39	1.81	77.57	22.43	0.29		
	ADTH 37	47.62	52.38	1.10	37.10	62.90	1.70	78.36	21.64	0.28		
	Means	61.34	38.66	0.67	40.97	59.04	1.48	79.58	20.42	0.26		
Wall-coating mortars	ADTH 7	59.50	40.50	0.68	38.66	61.34	1.59	75.22	24.78	0.33	70–80	1.5–3
	ADTH 31	54.62	45.39	0.83	40.12	59.88	1.49	79.22	20.78	0.26		
	ADTH 52	60.80	39.20	0.64	40.04	59.96	1.50	80.38	19.62	0.24		
	Menas	58.31	41.70	0.72	39.61	60.39	1.53	78.27	21.73	0.28		
Floor conglomerates (*rudus*)	ADTH 3	66.29	33.71	0.51	62.27	37.73	0.61	80.16	19.84	0.25	70–80	12.5–20
	ADTH 15	58.62	41.39	0.71	59.81	40.19	0.67	80.53	19.47	0.24		
	ADTH 25	65.60	34.40	0.52	45.46	54.54	1.20	84.12	15.88	0.19		
	ADTH 32	62.41	37.60	0.60	50.50	49.50	0.98	81.51	18.49	0.23		
	ADTH 33	62.27	37.73	0.61	48.55	51.45	1.06	83.57	16.43	0.20		
	Means	63.04	36.97	0.59	53.32	46.68	0.90	81.98	18.02	0.22		
Wall conglomerates (*trullisatio*)	ADTH 18	59.73	40.27	0.67	49.03	50.97	1.04	83.51	16.49	0.20	70–80	2.5–5
	ADTH 26	53.87	46.13	0.86	52.19	47.81	0.92	84.12	15.88	0.19		
	ADTH 58	64.17	35.83	0.56	60.97	39.03	0.64	78.76	21.24	0.27		
	Means	59.26	40.74	0.70	54.06	45.94	0.87	82.13	17.87	0.22		
Vault concretes	ADTH 12	62.80	37.20	0.59	36.02	63.98	1.78	80.58	19.42	0.24	70–80	>20
	ADTH 50	67.87	32.13	0.47	32.62	67.38	2.07	85.60	14.40	0.17		
	ADTH 53	64.05	35.96	0.56	37.44	62.56	1.67	82.81	17.19	0.21		
	Means	64.91	35.10	0.54	35.36	64.64	1.84	83.00	17.00	0.21		
Plasters	ADTH 13	60.48	39.52	0.65	53.40	46.60	0.87	81.68	18.32	0.22	65–70	1.5–2.5
	ADTH 14	61.49	38.51	0.63	49.39	50.61	1.02	80.01	19.99	0.25		
	Means	60.99	39.02	0.64	51.40	48.61	0.95	80.85	19.16	0.24		

Vitruvio's values of binder/aggregate ratio and mortar thickness are also reported

B binder, *A* aggregate

of a concentrated load with two opposing conical punches.

The resistance to puncturing (I_S) was calculated as P/D_e^2, where P is the breaking load and D_e is the "equivalent diameter of the carrot" (ISRM 1985), with $D_e = 4\ A/\pi$ and $A = W \times D$, where W and $2L$ are the width perpendicular to the direction of the load and the length of the specimen, respectively. The index value is referred to a standard cylindrical specimen with diameter $D = 50$ mm for which I_S has been corrected with a shape coefficient (F) and calculated as

$$I_{S(50)} = I_S \cdot F = I_S \cdot (D_e/50)^{0.45}$$

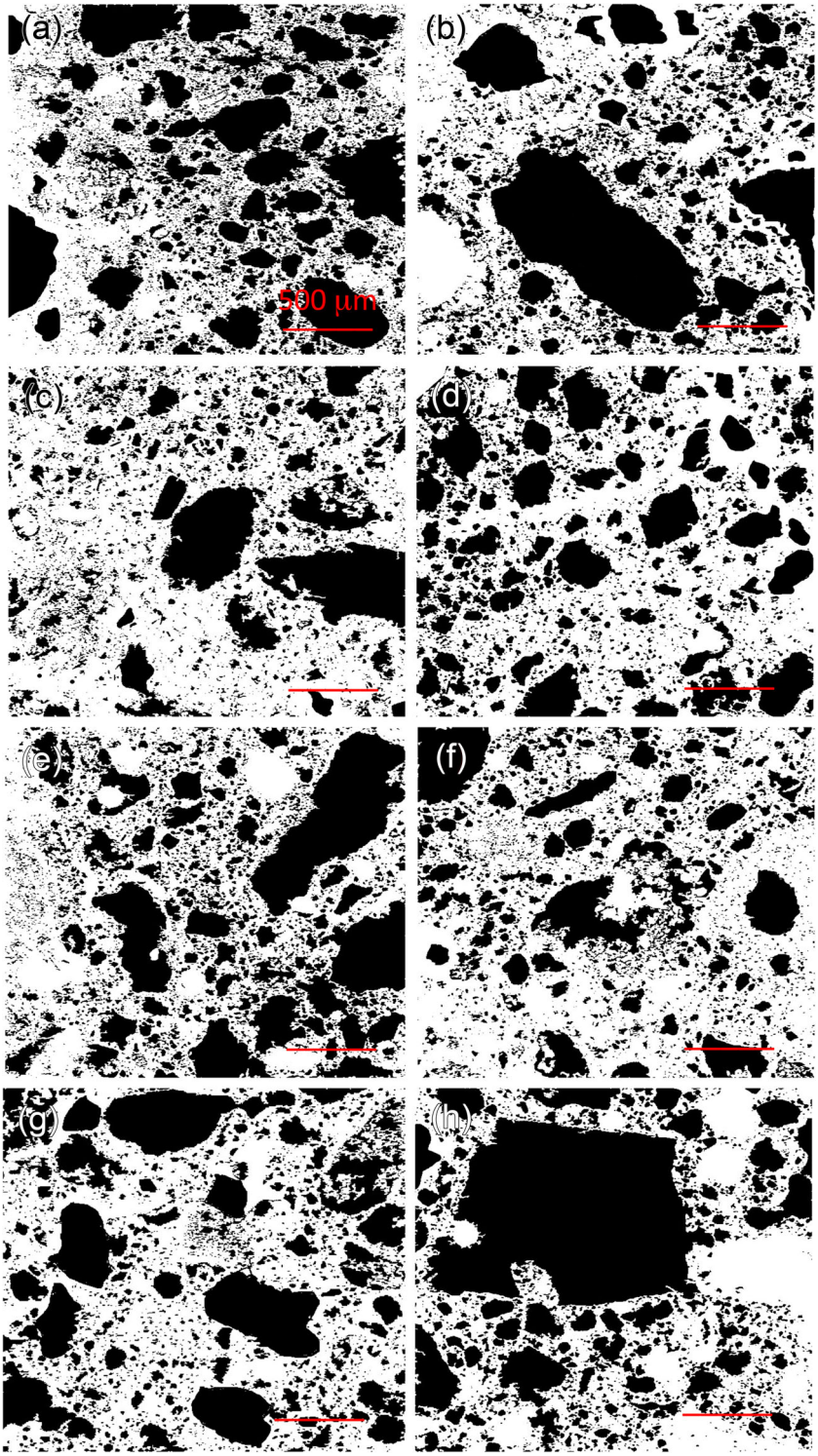

Fig. 5 Microphotographs on mortar thin section realized with binarization and filling holes options by image analysis with software ImageJ 1.47v. **a** Brick mortar; **b** *cubilia* mortar; **c** floor coating mortars; **d** wall coating mortar; **e** floor conglomerate; **f** wall conglomerate; **g** vault concrete; **h** plaster

The simple compression resistance (R_C) and the traction resistance (R_T) of the mortar were indirectly calculated (according to ISRM 1985) using the value of normalized punching resistance, each of them as

$$R_C = K \cdot I_{S(50)} \qquad R_T = I_{S(50)}/0.8$$

where K (multiplication coefficient) = 14 (Palmström 1995).

To proceed with the particle-size analysis, the mortars were first disaggregated with the use of a mortar and pestle, dried at 105 ± 5 °C, weighed to measure the dry mass (m_{dM}), and then attached with acid solution (HNO_3, 13 % vol.) for a period of immersion of 48 h, so as to eliminate the carbonate binder matrix of the mortar. The samples were then filtered with Whatman 41 paper, washed in distilled water, and placed in an oven at 105 ± 5 °C to determine the dry mass of the residual aggregate (m_{dR}) and, indirectly, the bulk mass of the binder (e.g., $m_{dB} = m_{dM} - m_{dR}$). Then, the particle-size distribution was performed using sieves with mesh opening of 6300, 4000, 2000, 500, 250, 125, and 63 μm with a Giuliani IG3 sifter.

Results and discussion

Mineralogical and petrographic characteristics

At the macroscopic observation, the binder matrix of samples shows a color from grayish (CIELAB 89*-1*4) to whitish (CIELAB 89*0*0) (on fresh cut). The surfaces exposed directly to the weathering, due to the alteration (decarbonation, sulfation), show a different color, from ochre (CIELAB 74*9*12) to gray more intense (CIELAB 51*1*5).

In the zones of the building exposed to the north, without sun radiation, biological patinas are present, with various species (e.g., molds, mosses, lichens).

In all mortars, there are often lime lumps with different dimensions (from <1 to 7 mm), in some cases with radial fissuring or fractured.

The binder matrix is mainly constituted by microcrystalline calcite (Fig. 4) in which the presence of microporosity finely distributed in the paste is observed.

Different gravel, sands, or crushed rocks were employed in the aggregate of mortars such as volcanic rocks (and subordinately marble), crystal-clasts, and *cocciopesto* fragments of bricks, tiles, and pottery. The latter were mainly used in the wall and floor conglomerates.

The mineralogical composition of the aggregate was defined by microscopic analysis in thin section, reported in Table 1.

In Table 2, irrespective of the composition, circularity data of aggregate are reported, determined with image analysis on thin-section photographs by software ImageJ 1.47v. The circularity of the aggregate with size <8 mm is substantially similar in the various kinds of mortar. Therefore, they were not counted as coarse fragments, frequently found in the vault concretes (e.g., *caementia*, with main size range 30–150 mm) and *cocciopesto* conglomerates of walls and floors (size range 10–30 mm). Counting this coarse aggregate, surely the circularity value would be considerably lower.

The volcanic aggregate is made from two kinds of rocks: leucitic basalt and leucitites, belonging to the alkaline rocks of ultrapotassic series (HKS) from the Roman Magmatic Province (Morbidelli 2003; Peccerillo 2005).

The first is mainly represented by two kinds of scoria clasts (Fig. 4) with different color: gray-black and gray-red. It has normally subspherical shape with porous and glassy appearance. Both types of leucitic basaltic aggregate are present in all mortar samples with high amounts (>65 %; Table 1) with respect to total aggregate. It shows great similarity with the volcanic scoria outcropping around Hadrian's Villa.

The texture of leucitic basalt is afiric. The paragenesis consists of clinopyroxene (Fig. 4), leucite, hornblende, opaque minerals (i.e., Ti-magnetite, magnetite), ±plagioclase. Rare biotite and olivine, often altered in iddingsite, are present. Having a glassy matrix, they show edge of pozzolanic reaction with the binder (Fig. 4).

The leucitite aggregate (Fig. 4) has a lower presence in the mortars with respect to leucitic basaltic scoria. It represents <8 % of total aggregate (Table 1). It has a grayish color with shape normally subspherical (Table 2), shows a low porosity, and is frequently altered. The paragenesis is mainly composed by leucite, clinopyroxenes, and opaque minerals, while the feldspars are rare or absent.

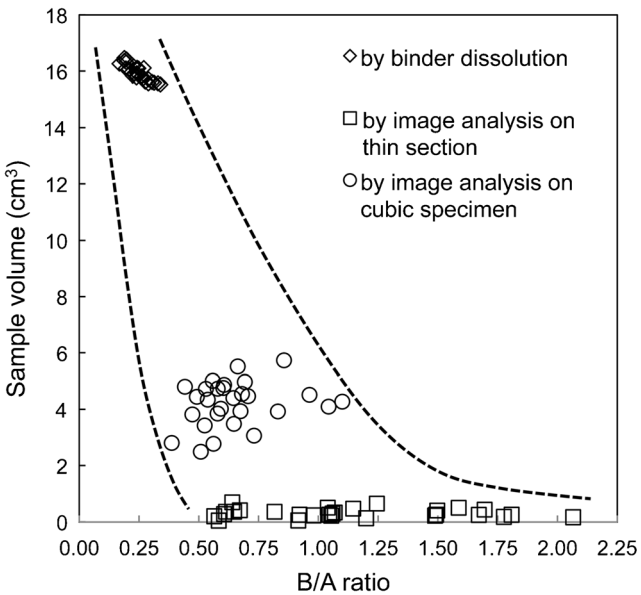

Fig. 6 Comparison of three different methods to calculate the binder/aggregate ratio (vol.%) using different sample volumes by image analysis on thin section and on cubic bulk mortar specimens, and using weight data from acid dissolution of binder mortar to determine the particle size analysis

Table 4 Comparison data of the aggregate ratio using the compositional distribution, determined by microscopic analysis, and weight data after dissolution of binder used for making the particle size analysis

Sample	Aggregate	Binder	B/A (wt)	Aggregate	Binder	Aggregate fragment/crystal weights (g)								Aggregate fragment/crystal volumes (cm^3)								Binder volume (cm^3)
	wt (g)			wt (%)		Sc	Le	CP	Mbl	Cpx	Hnb	Bt	Total	Sc	Le	CP	Mbl	Cpx	Hnb	Bt	Total	
ADTH 4	22.55	7.45	0.33	75.17	24.83	22.44	0.00	0.00	0.11	0.00	0.00	0.00	22.55	8.98	0.00	0.00	0.04	0.00	0.00	0.00	9.02	2.75
ADTH 6	22.39	7.61	0.34	74.63	25.37	22.19	0.16	0.00	0.04	0.00	0.00	0.00	22.39	8.87	0.07	0.00	0.02	0.00	0.00	0.00	8.97	2.81
ADTH 11	24.24	5.76	0.24	80.80	19.20	23.80	0.36	0.00	0.00	0.07	0.00	0.00	24.24	9.52	0.17	0.00	0.00	0.02	0.00	0.00	9.72	2.13
ADTH 21	23.24	6.77	0.29	77.45	22.55	23.19	0.00	0.00	0.05	0.00	0.00	0.00	23.24	9.28	0.00	0.00	0.02	0.00	0.00	0.00	9.29	2.50
ADTH 35	24.00	6.00	0.25	80.01	19.99	22.63	0.91	0.00	0.00	0.46	0.00	0.00	24.00	9.05	0.43	0.00	0.00	0.13	0.00	0.00	9.62	2.21
ADTH 42	23.64	6.36	0.27	78.79	21.21	22.88	0.26	0.00	0.02	0.21	0.26	0.00	23.64	9.15	0.12	0.00	0.01	0.06	0.08	0.00	9.43	2.35
ADTH 43	23.42	6.58	0.28	78.08	21.92	23.28	0.00	0.00	0.14	0.00	0.00	0.00	23.42	9.31	0.00	0.00	0.05	0.00	0.00	0.00	9.37	2.43
ADTH 23	24.76	5.24	0.21	82.53	17.47	24.73	0.00	0.00	0.02	0.00	0.00	0.00	24.76	9.89	0.00	0.00	0.01	0.00	0.00	0.00	9.90	1.93
ADTH 46	22.83	7.17	0.31	76.10	23.90	22.33	0.18	0.00	0.05	0.27	0.00	0.00	22.83	8.93	0.09	0.00	0.02	0.08	0.00	0.00	9.12	2.65
ADTH 54	21.94	8.06	0.37	73.12	26.88	20.99	0.46	0.00	0.07	0.26	0.15	0.00	21.94	8.40	0.22	0.00	0.02	0.08	0.05	0.00	8.77	2.98
ADTH 24	24.12	5.88	0.24	80.41	19.59	23.01	0.00	1.04	0.00	0.00	0.07	0.00	24.12	9.21	0.00	0.46	0.00	0.00	0.02	0.00	9.69	2.17
ADTH 28	23.84	6.16	0.26	79.48	20.52	20.96	0.24	1.22	0.00	0.24	0.95	0.24	23.84	8.38	0.11	0.54	0.00	0.07	0.30	0.08	9.49	2.27
ADTH 34	22.81	7.19	0.32	76.03	23.97	21.71	0.00	1.09	0.00	0.00	0.00	0.00	22.81	8.69	0.00	0.49	0.00	0.00	0.00	0.00	9.17	2.65
ADTH 37	23.07	6.93	0.30	76.89	23.11	21.94	0.00	1.04	0.00	0.09	0.00	0.00	23.07	8.77	0.00	0.46	0.00	0.03	0.00	0.00	9.27	2.56
ADTH 7	22.13	7.87	0.36	73.78	26.22	21.69	0.00	0.00	0.00	0.22	0.22	0.00	22.13	8.68	0.00	0.00	0.00	0.07	0.07	0.00	8.81	2.90
ADTH 31	23.36	6.64	0.28	77.87	22.13	22.96	0.19	0.00	0.00	0.00	0.21	0.00	23.36	9.19	0.09	0.00	0.00	0.00	0.07	0.00	9.34	2.45
ADTH 52	23.73	6.27	0.26	79.11	20.89	23.57	0.00	0.00	0.00	0.17	0.00	0.00	23.73	9.43	0.00	0.00	0.00	0.05	0.00	0.00	9.48	2.31
ADTH 3	23.58	6.42	0.27	78.60	21.40	20.21	0.00	3.25	0.00	0.12	0.00	0.00	23.58	8.08	0.00	1.45	0.00	0.03	0.00	0.00	9.57	2.37
ADTH 15	23.70	6.30	0.27	79.00	21.00	20.83	0.00	2.87	0.00	0.00	0.00	0.00	23.70	8.33	0.00	1.28	0.00	0.00	0.00	0.00	9.61	2.32
ADTH 25	24.83	5.18	0.21	82.75	17.25	19.81	0.79	3.77	0.00	0.45	0.00	0.00	24.83	7.92	0.38	1.68	0.00	0.13	0.00	0.00	10.12	1.91
ADTH 32	23.94	6.06	0.25	79.81	20.19	18.84	1.22	3.88	0.00	0.00	0.00	0.00	23.94	7.54	0.58	1.73	0.00	0.00	0.00	0.00	9.85	2.24
ADTH 33	24.65	5.35	0.22	82.17	17.83	19.97	0.52	3.77	0.00	0.00	0.39	0.00	24.65	7.99	0.25	1.68	0.00	0.00	0.13	0.00	10.04	1.97
ADTH 18	24.57	5.43	0.22	81.91	18.09	17.96	1.89	4.35	0.00	0.22	0.15	0.00	24.57	7.19	0.90	1.94	0.00	0.07	0.05	0.00	10.14	2.00
ADTH 26	24.79	5.21	0.21	82.62	17.38	18.96	0.67	5.06	0.00	0.00	0.10	0.00	24.79	7.58	0.32	2.26	0.00	0.00	0.03	0.00	10.19	1.92
ADTH 58	23.12	6.88	0.30	77.06	22.94	19.67	0.25	3.19	0.00	0.00	0.00	0.00	23.12	7.87	0.12	1.42	0.00	0.00	0.00	0.00	9.41	2.54
ADTH 12	23.78	6.22	0.26	79.28	20.72	23.43	0.21	0.00	0.02	0.00	0.12	0.00	23.78	9.37	0.10	0.00	0.01	0.00	0.04	0.00	9.52	2.29
ADTH 50	25.39	4.61	0.18	84.62	15.38	25.06	0.00	0.00	0.03	0.30	0.00	0.00	25.39	10.02	0.00	0.00	0.01	0.09	0.00	0.00	10.12	1.70
ADTH 53	24.49	5.51	0.23	81.63	18.37	24.44	0.00	0.00	0.05	0.00	0.00	0.00	24.49	9.78	0.00	0.00	0.02	0.00	0.00	0.00	9.79	2.03
ADTH 13	24.06	5.94	0.25	80.21	19.79	20.31	1.25	1.97	0.00	0.00	0.53	0.00	24.06	8.12	0.60	0.88	0.00	0.00	0.17	0.00	9.77	2.19
ADTH 14	23.53	6.47	0.27	78.44	21.56	19.23	0.00	3.91	0.00	0.33	0.07	0.00	23.53	7.69	0.00	1.74	0.00	0.10	0.02	0.00	9.55	2.39

B binder, *A* aggregate

The crystal-clasts of mortar aggregate essentially consist of hornblende, clinopyroxene, and rare biotite.

The *cocciopesto* aggregate (Fig. 4; Tables 1 and 2) has variable size of fragments with angular shape. It has a variable color from yellow-ochre to pink-orange to rust-red, due to different compositions and fire conditions. Consequently, these ceramic products show variable physical characteristics (porosity, mechanical strength; Columbu et al. 2015b). *Cocciopesto* aggregate shows typical edge of reaction with binder (Fig. 4). Observing the matrix, crystals of quartz and plagioclase immersed into the matrix are present. Rare leucitic basaltic fragments (<5 % in total) and Fe-oxides (e.g., hematite) are present.

The mortar samples show the occasional presence (in low amount) of white marble aggregate, normally with sharp edges. This aggregate is mainly present in the finishing lime plasters and, subordinately, in the bedding mortars of *cubilia*, brick walls, and vault concretes.

In some samples, local pyroclastic rocks (belonging to Hadrian's Villa area) were used as coarse aggregate or *caementia* in the concretes (with frequent size 5–20 cm). This rock is characterized by a glassy groundmass, lithic-clasts of varying particle size with composition from leucitic-basaltic to leucititic xenoliths (Fig. 4). Occasionally, it shows typical alterations in zeolites and clay minerals (Peccerillo 2005). The accessory phases are

Table 5 Data used for making the graphic of Fig. 6, where binder/aggregate ratio (determine by volume) and specimen volume (cm^3) are reported

Mortar typology	Sample	Binder/aggregate ratio (by volume)			Specimen volume (cm^3)		
		By image analysis on cubic specimens	By image analysis on thin section	By binder dissolution	Cubic specimen	Thin section	Dissolution
Brick bedding mortars	ADTH 4	0.58	0.58	0.30	4.73	0.05	15.62
	ADTH 6	0.53	0.82	0.31	4.73	0.35	15.59
	ADTH 11	1.04	0.56	0.22	4.09	0.20	15.96
	ADTH 21	0.69	0.65	0.27	4.97	0.35	15.76
	ADTH 35	0.39	0.61	0.23	2.80	0.35	15.92
	ADTH 42	0.96	1.49	0.25	4.51	0.22	15.85
	ADTH 43	0.66	0.92	0.26	5.51	0.25	15.80
Cubilia bedding mortars	ADTH 23	0.49	1.05	0.34	4.44	0.25	16.10
	ADTH 46	0.73	1.07	0.29	3.06	0.33	15.71
	ADTH 54	0.65	1.05	0.20	3.48	0.22	15.53
Floor-coating bedding mortars	ADTH 24	0.58	1.15	0.22	3.85	0.46	15.84
	ADTH 28	0.44	1.24	0.24	4.80	0.65	15.78
	ADTH 34	0.54	1.81	0.29	4.34	0.25	15.57
	ADTH 37	1.10	1.70	0.28	4.27	0.43	15.63
Wall-coating mortars	ADTH 7	0.68	1.59	0.33	4.54	0.49	15.57
	ADTH 31	0.83	1.49	0.26	3.92	0.25	15.82
	ADTH 52	0.64	1.50	0.24	4.40	0.40	15.90
Floor conglomerates (*rudus*)	ADTH 3	0.51	0.61	0.25	2.49	0.28	16.10
	ADTH 15	0.71	0.67	0.24	4.46	0.41	16.12
	ADTH 25	0.52	1.20	0.19	3.42	0.13	16.37
	ADTH 32	0.60	0.98	0.23	4.76	0.23	16.18
	ADTH 33	0.61	1.06	0.20	4.87	0.29	16.32
Wall conglomerates (*trullisatio*)	ADTH 18	0.67	1.04	0.20	3.93	0.50	16.42
	ADTH 26	0.86	0.92	0.19	5.73	0.05	16.47
	ADTH 58	0.56	0.64	0.27	5.01	0.69	16.11
Vault concretes	ADTH 12	0.59	1.78	0.24	4.02	0.18	15.93
	ADTH 50	0.47	2.07	0.17	3.82	0.17	16.26
	ADTH 53	0.56	1.67	0.21	2.77	0.25	16.07
Plasters	ADTH 13	0.65	0.87	0.22	5.77	0.65	16.32
	ADTH 14	0.63	1.02	0.25	5.92	0.12	16.20

iron and titanium oxides. Due to volcanic glass, the pyroclastites were probably used also as pozzolanic aggregate. In the aggregate of mortars, the presence of the same crystal-clasts, observed in the same pyroclastic rock, has been frequently detected (i.e., green hornblende, clinopyroxene, biotite) as well as the leucitic basalt and leucitites.

Binder/aggregate ratio

According to Columbu et al. (2015b), the ratio of binder and aggregate was initially calculated through the image analysis on the six faces of the cubic specimens. The values are reported in Table 3 (first three columns).

The results show that this ratio depending varies on the specific function of the mortar in the baths. The average values for mortar group are higher in mortars with low thickness: wall *cocciopesto* conglomerates of *trullisatio* layer (0.70; Table 3) and brick mortars (0.68). Instead, in the mortars of vault concretes and floor *cocciopesto* conglomerates (*rudus*), the average values are lower (0.54 and 0.59, respectively) due to higher presence of medium-coarse aggregate.

However, this binder/aggregate ratio also varies within the sample groups, showing a certain compositional inhomogeneity in the preparation of mortars.

For comparison, the mixing ratio between binder and aggregate has also been obtained through image analysis of photographs taken under a microscope (Table 3; Fig. 5). The values are always higher than those obtained by image analysis of cubic specimens (Table 3) due to different volumes of samples analyzed in the two cases (Fig. 6).

In both cases, the values are higher than the values indicated by *Vitruvio* (Pollione 15 BC). According to his recommendations (Table 3), the aggregate percentage in a mortar is mainly a function of particle size distribution and the thickness of the mortar cast. So, a thickness of 1–2 cm provides an aggregate percentage of 65–70 vol.%, while a thickness >2 cm provides an aggregate percentage of 70–80 vol.% (Cagnana 2000).

Based on the results obtained with both methods, the percentage of aggregate more similar to the recommendations of *Vitruvio* is the one obtained by image analysis on cubic specimens (Table 3), but this is not perfectly correct because it does not detect the presence of aggregate with very small size (<100 μm) undetectable by the image analysis.

Further values were calculated using weight ratio data (Table 4) after binder dissolution of the mortars made to determine the particle size of aggregate, where all aggregate fraction is counted, even those less than 100 μm in diameter. Data (Table 4) are very close to those recommended by Vitruvius (Table 3). So, the latter method shows higher reliability than the other due to a larger volume of the samples (Table 5), as shown in Fig. 6.

Composition of binder

XRPD and TG/DSC analyses on the fractions enriched in binder have provided information on the materials used and the main, secondary, and reactant phases between binder and aggregate, allowing us to define the composition and hydraulic degree of the mortars.

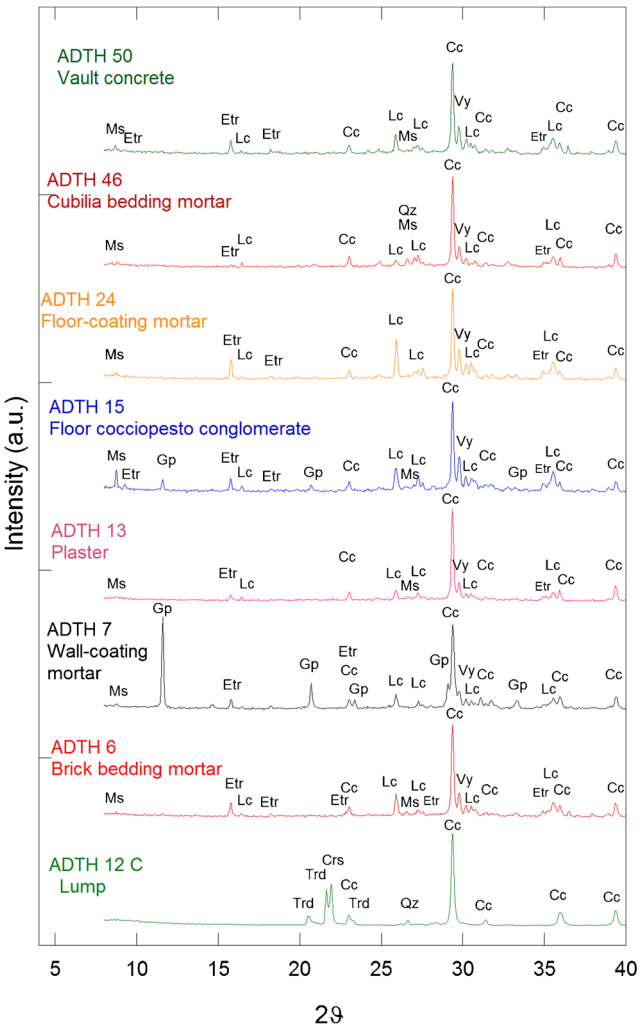

Fig. 7 Qualitative mineralogical analysis of binder. XRPD patterns of selected samples of aerial and hydraulic mortars. The *dotted curves* are the experimental data. The reflection positions of major components are shown: Tridimite (PDF card 18-1170), Crystobalite (PDF card 71-785), Quartz (PDF card 79-1906), Calcite (PDF card 5-586), Gypsum (PDF card 21-816), Leucite (PDF card 71-1147), Muscovite (PDF card 7-25), Ettringite (PDF card 41-1451), and Vuagnatite (PDF card 29-289) phases. Mineral abbreviations: *Cc* calcite, *Qz* quartz, *Crd* cristobalite, *Trd* tridymite, *Gp* gypsum, *Lc* leucite, *Ms* muscovite, *Etr* ettringite, *Vy* vuagnatite

Selected samples were analyzed by x-ray powder diffraction, and patterns are shown in Fig. 7. In all samples, the main Bragg reflections match with the database values for calcite ($CaCO_3$) phase. For ADTH 12C sample, in addition, peaks (at 20.50, 21.63, and 23.29 2ϑ degrees) due to tridymite, peaks (at 21.96 and 28.42 2ϑ degrees) due to cristobalite, and peaks due to quartz were also observed. Tridymite and cristobalite phases were not observed in the XRDP of the other samples. In these samples, leucite ($KAlSi_2O_6$) and muscovite ($KAl_2Si_3AlO_{10}(OH)_2$) phases were also observed. Other minor phases of syngenite ($K_2Ca(SO_4)_2{\cdot}H_2O$) and quartz are also present. Quartz, leucite, and mica (i.e., muscovite) belong to the phases of aggregate, from volcanic rocks (scoria and leucitite) and crystal-clasts.

In the XRDP patterns of ADTH 7 and ADTH 15 samples, peaks due to gypsum ($CaSO_4{\cdot}2H_2O$) phase were present; in ADTH 7 sample, peaks due to gypsum are very intense. Gypsum is due to sulfation processes, facilitated by the high open porosity calculated on the binder matrix.

Owing to the reactions between the binder and the pozzolan materials, between the hydraulic phases of new formation, only a small amount of an Ca/Al-silicate [i.e., vuagnatite ($CaAlSiO_4(OH)$)] and ettringite ($Ca_6A_{12}(SO)_4(OH)_{12}{\cdot}26H_2O$) have been identified in all samples (excluding ADTH 12C) by x-ray diffraction. The products of the pozzolanic reaction probably are mainly present as amorphous phases (gel-like C-S-A-H). Ettringite is formed as a consequence of the chemical reaction between the sulfates and aluminates usually present in the hydration products of Portland cement. Its formation depends on different factors: (1) aluminates content, (2) amount and origin of sulfates, and (3) quality of the mortar. Then, ettringite crystallization involves a high increment of volume due to an expansive process with mortar disintegration (cracking and loss of mass).

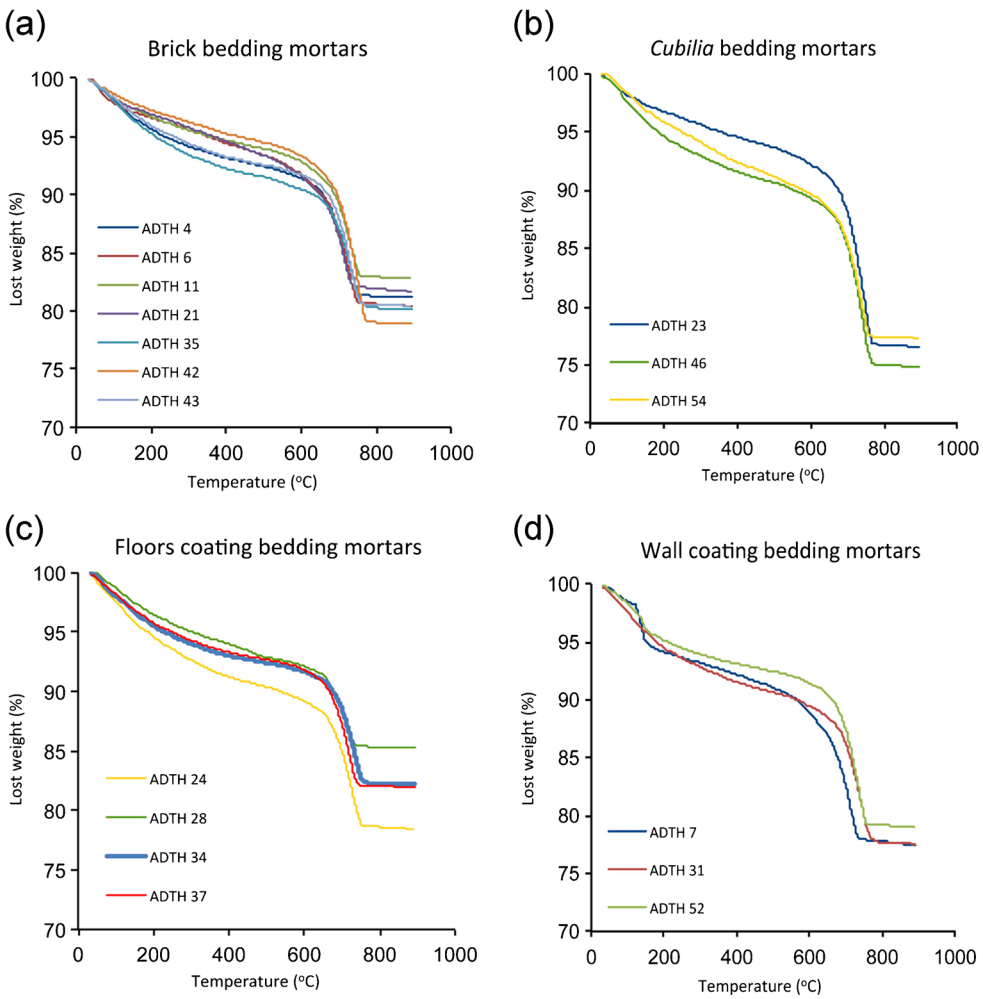

Fig. 8 Thermogravimetric analysis on the enriched binder fraction of mortars. TG curves: mass loss (%) versus temperature in degrees Celsius. **a** Brick mortar; **b** *cubilia* mortar; **c** floor coating mortars; **d** wall coating mortar. Thermogravimetric analysis on the enriched binder fraction of mortars. TG curves: mass loss (%) versus temperature in degrees Celsius. **e** Floor conglomerate; **f** wall conglomerate; **g** vault concrete; **h** plaster; **i** lump

The curves obtained with the TG/DSC simultaneous analysis (Figs. 8 and 9) have a typical trend of pozzolanic mortars (according to Branda et al. 2001). The curves show an initial loss of weight due to hygroscopic water below 120 °C (Table 6). The observed gypsum phase in these XRDP patterns is in agreement with the TGA result, where a net jump at 122–150 °C due to crystallized water loss of this phase is present in TGA curves of these samples. A following weight loss is present at temperatures between 480 and 500 °C, probably associated with the reaction between calcium silicates and carbonates which liberate carbon dioxide according to the following chemical reaction:

$$CaCO_3 + XSiO_2 \Rightarrow CaXSiO_3 + CO_2 (where\ X = K, Al, F)$$

The more extensive loss in weight is recorded on the decomposition curve at temperatures between 550 and 600 °C and 800–830 °C and is linked to the decarbonation reaction of Ca-carbonate ($CaCO_3 \Rightarrow CaO + CO_2$). From the curves, it is observed that not all the samples have similar extension of the weight loss, showing a discrete compositional heterogeneity. The losses in weight percentages related to the elimination of H_2O and CO_2 compounds (evaporation and decarbonation) are useful to trace pozzolanic activity of the analyzed sample.

The endothermic peaks (Fig. 9) of calorimetric curves (DSC) coincide with temperatures at which losses in weight in the TG curves are observed. Although the general meaning of different trends in thermic curves has not yet been clarified

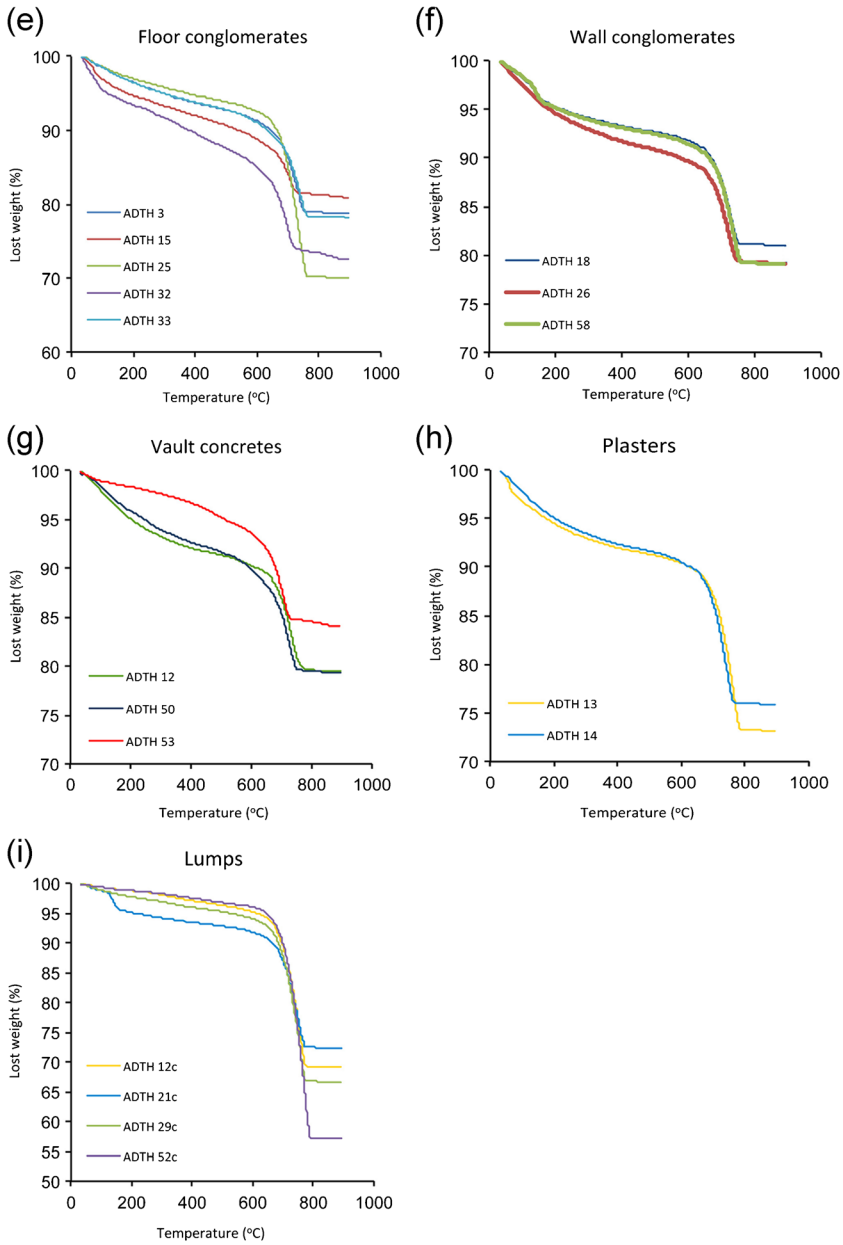

Fig. 8 (continued)

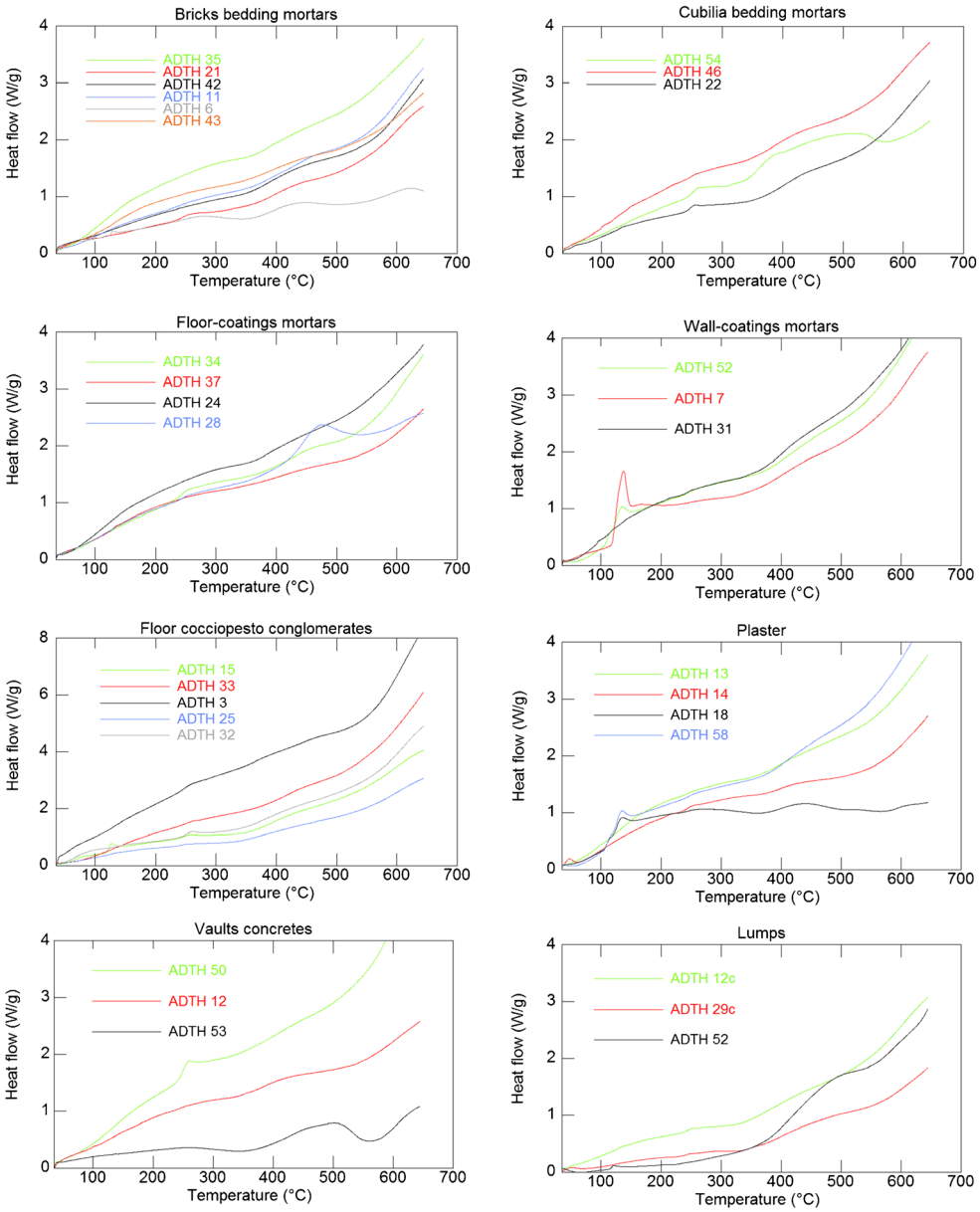

Fig. 9 Differential scanning calorimetric (DSC) curves related to the enriched binder fraction of mortars. Heat flow versus temperature

exhaustively, the losses in weight from low temperatures (~400 °C) are due to reactions between calcium carbonate and silicates with formation of calcium silicates and production of CO_2.

In DSC curves, it is noteworthy that in the samples containing gypsum (wall-coating mortars ADTH 7, ADTH 52; floor *cocciopesto* conglomerates ADTH 15, plaster ADTH 18, ADTH 58), an endothermic sharp peak due to dehydration of gypsum is observed.

In some samples, in the range 480–500 °C, it is observed that there is a broad endothermic peak (evident in ADTH 28 sample) due to the reaction between calcite and silicate to form Ca-silicate that develops carbon dioxide. This reaction may be also due to the presence of new cement mortar residues of the restoration interventions in the last decades.

Finally, at higher temperatures (>600 °C) in all the samples, the DSC curves have shown an increasing upward behavior due to the incipient endothermic decomposition of calcite.

According to temperature ranges with characteristic losses in weight identified by Bakolas et al. (1995, 1998) and Moropoulou et al. (2000), CO_2 versus CO_2/H_2O ratio has been reported in Fig. 10, where CO_2 is weight loss between 600 and 800 °C and H_2O is weight loss of bond water in the range of 200–600 °C (Table 7). Samples with greater hydraulic degree are the mortars of marble flooring (CO_2 = 9.79 %), followed by the vault

Table 6 Thermogravimetric analysis: percentage weight difference data of enriched binder samples in the following temperature ranges: 25–120, 120–200, 200–400, 400–600, 600–850 °C

Mortar typology	Sample	Δw (%) 25–120 °C	Δw (%) 120–200 °C	Δw (%) 200–400 °C	Δw (%) 400–600 °C	Δw (%) 600–850 °C
Brick bedding mortars	ADTH 4	2.5	1.9	2.4	1.8	10.2
	ADTH 6	2.5	0.9	2.2	2.8	11.1
	ADTH 11	2.1	1.2	2.2	1.7	10.9
	ADTH 21	2.1	0.9	2.5	2.9	9.8
	ADTH 35	2.5	2.3	3.0	1.8	10.3
	ADTH 42	1.7	1.0	2.1	1.9	14.4
	ADTH 43	2.3	1.7	2.8	1.6	11.1
Cubilia bedding mortars	ADTH 23	2.1	1.1	2.2	2.4	15.6
	ADTH 46	4.0	1.4	3.0	2.3	14.4
	ADTH 54	2.3	1.8	3.5	2.7	12.4
Floor-coating bedding mortars	ADTH 24	3.2	2.2	3.4	2.1	10.6
	ADTH 28	1.7	1.9	2.4	1.9	6.8
	ADTH 34	2.6	1.9	2.5	1.3	9.5
	ADTH 37	2.4	1.8	2.5	1.5	9.9
Wall-coating mortars	ADTH 7	1.7	4.2	1.9	3.3	11.3
	ADTH 31	3.2	2.3	3.0	2.1	11.8
	ADTH 52	2.3	2.6	2.0	1.7	12.3
Floor conglomerates (*rudus*)	ADTH 3	1.9	1.6	2.7	2.6	12.3
	ADTH 15	3.5	1.8	2.7	3.3	7.6
	ADTH 25	1.7	1.3	2.2	2.2	21.7
	ADTH 32	5	1.5	3.9	4.6	12.2
	ADTH 33	1.9	1.6	2.6	2.9	12.7
Wall conglomerates (*trullisatio*)	ADTH 18	2.4	2.3	2.0	1.5	10.7
	ADTH 26	3.1	2.3	2.9	2.1	10.5
	ADTH 58	2.3	2.7	1.8	1.8	12.3
Vault concretes	ADTH 12	2.7	2.2	3.0	1.7	11.0
	ADTH 50	2.2	2.0	3.2	2.7	10.5
	ADTH 53	1.7	0.5	1.6	3.2	9.3
Plasters	ADTH 13	2.9	2.1	2.7	1.8	14.6
	ADTH 14	3.5	1.7	2.5	1.5	16.1
	ADTH 12C	0.7	0.5	1.6	2.1	25.9
Lumps	ADTH 29C	1.4	0.8	1.8	2.0	27.4
	ADTH 52C	0.7	0.5	1.3	1.5	38.8

concretes (CO_2 = 11.25 %), *arriccio* plasters (CO_2 = 11,65 %), brick bedding mortars (CO_2 = 12.34 %), and the coating bedding mortars (CO_2 = 12.74 %). The lime lumps, being mainly compounds of Ca-hydroxide/carbonate, have much higher values. The diagram shows an exponential correlation of data (R^2 = 0.95; Fig. 10).

Particle size analysis of aggregate

The analysis of determinant diameters D_{10} and D_{60} in cumulative distribution curves, obtained by sieving of the aggregate fraction (Fig. 11; Table 8), shows that 77 % of the analyzed mortars present a poorly sorted particle size distribution, 13 % of mortars present a varied particle size distribution (samples ADTH 6, 43, 18, 50), and the last 10 % present a sorted particle size distribution (samples ADTH 23, 3, 13).

According to size classification (Wentworth 1922), cumulative curves (Fig. 11a–h) show how the aggregates are used in the mortars derived in most cases from very fine gravel aggregate (also call granule), where the histograms of hold masses record the highest percentages at about 4000 and 2000 μm grain size sieves (Columbu et al. 2015b). In other cases, where the frequency histogram recorded the highest held percentages on 2000 and

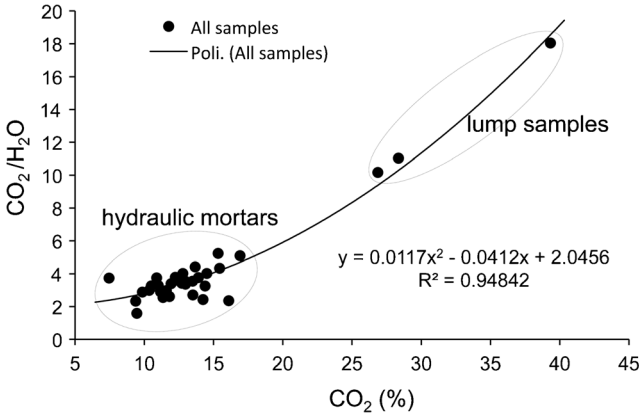

Fig. 10 Diagram of CO_2 versus CO_2/H_2O ratio for mortars of *Heliocaminus* Baths, where CO_2 is weight loss (%) between the temperature range of 600 and 800 °C and H_2O is weight loss of bond water in the range of 200–600 °C (from Moropoulou et al. 2000, modified)

1000 μm, these aggregates are defined as very coarse sand.

Granule aggregate is used in 74 % of the mortars. The remaining 26 % show an aggregate of very coarse sand.

The aggregate particle size is a function of mortar's thickness and percentage of inert aggregate used in the casting, parameters that are constant within the same group of mortars.

According to Columbu et al. (2015b), the slight variations in grain size within a same group would be attributable to unintentional different mixing of raw materials or different packaging modality probably due to the change of workers.

Some variations, such as those mentioned above, occur in the ADTH 53 sample (vault concretes) that shows granule particle size different from very fine gravel of ADTH 50 and ADTH 12 samples.

On the basis of cumulative curve morphology, each mortar group reflects a particular pattern even though in some cases it is different due to slightly dissimilar particle size characteristics (Fig. 11a–h). This is the example of brick bedding mortars (Fig. 11a) where the ADTH 4 and ADTH 42 samples deviate from the trend of other distribution curves. In these samples, the histograms indicate a modal class of 1000 and 2000 μm. The same behavior occurs in the wall coating and floor coating mortars (Fig. 11c, d) where ADTH 28, ADTH 37, and ADTH 7 samples slightly deviate from the trend of the other mortars. In these samples, the histograms indicate a modal class of 2000 and 1000 μm.

Floor conglomerates (Fig. 11e) show a fairly similar morphology of the cumulative curves with the exception of the ATDH 3 sample, which is characterized by a slight gap.

In vault concretes, there is a great similarity of the cumulative curves that appear superimposed (Fig. 11g).

The same morphological homogeneity of cumulative curves characterizes the plasters.

Physical-mechanical properties of mortars

Porosity, density, and water absorption

The following physical and mechanical properties of bulk mortar samples (according to Columbu et al. 2015b) are reported in Table 9: solid, real and bulk density**,** open and closed porosity to helium and water, weight imbibition coefficient, saturation index, and punching strength index. Physical properties of binders (calculated in a theoretical way) and aggregates are reported in Table 10.

The physical properties show value dispersion due to the different binder/aggregate mixture and relation between the size of aggregate and dimensions of bulk mortar specimens.

The porosity and bulk density are normally well correlated between them in inverse proportion, and they are good parameters to recognize the compactness degree of a mortar and also a good lay on the monument. Helium open porosity of mortars varies from 34.1 to 52.0 % and bulk density from 1.21 to 1.57 g/cm^3 (Table 9).

As highlighted in Fig. 12a, the great variability of helium open porosity and bulk density in the mortars is also affected by variable incidence of the binder and aggregate (Table 10). These properties range from 15.8 to 51.1 % and from 0.38 to 1.61 g/cm^3 in the binders, respectively, and from 13.7 to 48.0 % and from 1.40 to 2.20 g/cm^3 in the aggregate samples (Table 10). The binders also show a high variability of real density (Fig. 12b, Table 10). Considering that the solid density of binder (about 2.80 g/cm^3, corresponding to carbonate-lime phases) remains unchanged, it follows that the real density is influenced by the closed porosity present in the binder matrix and less by its solid density.

Observing the mean values (Tables 9 and 10), the samples of plasters and *cocciopesto* conglomerates of wall and floors show low values of open porosity (38.1 % and 42.1–43 %, respectively) than other mortars (ranging from 45 to 48 %). Bulk density shows values of 1.54 ± 0.01 g/cm^3, 1.50 ± 0.07 g/cm^3, and 1.34 ± 0.13 g/cm^3 in the plasters and in the conglomerates of floor and wall, respectively.

In the case of plasters (*arriccio* layer) and wall conglomerates (*trullisatio* layer), considering the low thickness (about 1 and 3 cm, respectively), the low porosity and high bulk density are due mainly to the pressing and working with plastering trowel during the laying. Moreover, in the plaster, this is also due to the use of a fine aggregate with respect to other mortars.

Table 7 Thermogravimetric analysis data of the mortars, where mass losses (%) for temperature ranges are reported

Mortar typology	Samples	Weight loss for temperature range (%)		CO_2/H_2O
		200–520 °C (H_2O)	520–800 °C (CO_2)	
Brick bedding mortars	ADTH 4	3.80	13.49	3.55
	ADTH 6	3.46	12.55	3.63
	ADTH 11	2.90	10.89	3.76
	ADTH 21	3.84	11.17	2.91
	ADTH 35	3.35	11.01	3.29
	ADTH 42	2.93	15.33	5.23
	ADTH 43	3.51	11.93	3.40
Cubilia bedding mortars	ADTH 23	3.32	16.91	5.09
	ADTH 46	4.42	14.39	3.26
	ADTH 54	4.98	13.51	2.71
Floor-coating bedding mortars	ADTH 24	4.44	11.35	2.56
	ADTH 28	1.99	7.45	3.74
	ADTH 34	3.42	9.86	2.88
	ADTH 37	3.22	10.50	3.26
Wall-coating mortars	ADTH 7	3.68	13.00	3.53
	ADTH 31	3.85	12.97	3.37
	ADTH 52	3.23	12.24	3.79
Floor conglomerates (*rudus*)	ADTH 3	3.69	13.91	3.77
	ADTH 15	4.02	9.38	2.33
	ADTH 25	3.09	13.67	4.42
	ADTH 32	5.86	14.24	2.43
	ADTH 33	3.61	14.51	4.02
Wall conglomerates (*trullisatio*)	ADTH 18	5.96	9.46	1.59
	ADTH 58	3.18	12.78	4.02
	ADTH 26	3.71	12.71	3.43
Vault concretes	ADTH 12	3.89	11.59	2.98
	ADTH 50	4.52	11.82	2.62
	ADTH 53	3.46	10.35	2.99
Plasters	ADTH 13	3.56	15.44	4.34
	ADTH 14	6.83	16.10	2.36
Lumps	ADTH 12C	2.64	26.86	10.17
	ADTH 29C	2.57	28.35	11.03
	ADTH 52C	2.18	39.33	18.04

The CO_2 (and H_2O) values were obtained using the TG curves, considering the temperature range in which the decarbonation reaction occurs

In the case of floor conglomerates, considering their structural function, the low porosity and more high bulk density with respect to wall conglomerates are due to a high and better compaction of mortar through the use of maces, as highlighted by different characteristics of the binders, with bulk density and total porosity of 0.77 ± 0.17 g/cm^3 vs. 0.64 ± 0.04 g/cm^3 and 51.8 ± 1.8 % vs. 63.4 ± 4.9 %, respectively (Table 10). These different physical properties of floor conglomerates are also due to a probable use of *cocciopesto* aggregate with higher quality, characterized by lower porosity and greater bulk density (Fig. 12a; samples ADTH 25C and ADTH 11C in Table 10).

Differently from other mortars described above, the vault concretes and the floor and wall bedding coating mortars show high He open porosity values (46.5 ± 3.3 %, 46.1 ± 3.5 %, and 47.8 ± 3.8 %, respectively; Table 9). In the first case, the thickness of the casting is probably due to a lower compaction or high amount of mixing water in the production of mortar, while in the case of coating mortars, it is due to the need to have a soft bedding mortar (therefore highly

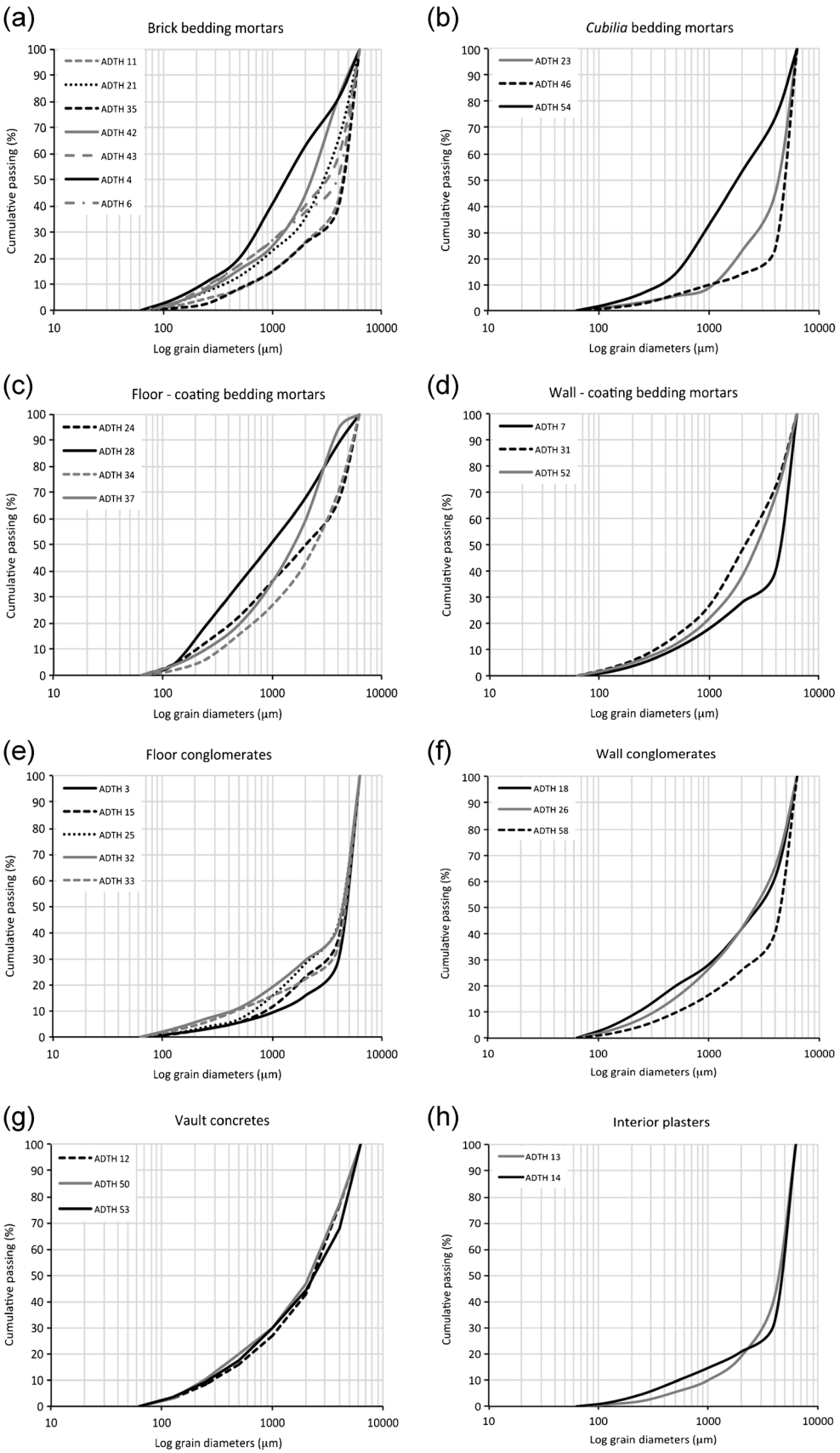

Fig. 11 Particle-size distribution of each mortar group with different functions in the *Heliocaminus* Baths. Log grain diameter versus cumulative passing percent

Table 8 Particle size analysis of aggregate: data of percentage cumulative passing to the following sieve series: 125, 250, 500, 1000, 2000, 4000, 6300 μm

Mortar typology	Sample	Cumulative passing (%)						
		6300 μm	4000 μm	2000 μm	1000 μm	500 μm	250 μm	125 μm
Brick bedding mortars	ADTH 4	100	81.0	62.9	40.8	20.2	10.9	4.2
	ADTH 6	100	50.9	37.6	26.9	17.4	9.4	2.7
	ADTH 11	100	42.0	26.2	15.1	8.1	4.5	1.5
	ADTH 21	100	64.9	35.4	22.9	13.1	7.2	2.7
	ADTH 35	100	39.2	25.8	15.0	8.4	2.5	0.8
	ADTH 42	100	81.1	44.2	24.7	15.7	7.7	2.8
	ADTH 43	100	58.5	40.1	26.8	17.5	8.7	2.3
Cubilia bedding mortars	ADTH 23	100	45.0	23.0	8.7	5.6	3.2	1.4
	ADTH 46	100	24.0	14.1	9.9	6.1	2.7	1.0
	ADTH 54	100	73.9	53.2	32.8	14.3	6.7	2.6
Floor-coating bedding mortars	ADTH 24	100	66.4	49.7	36.0	22.6	12.6	4.2
	ADTH 28	100	88.5	67.7	50.9	35.2	19.2	4.1
	ADTH 34	100	69.9	42.9	26.8	15.7	6.2	1.9
	ADTH 37	100	94.1	59.1	35.7	19.6	10.0	3.8
Wall-coating bedding mortars	ADTH 7	100	39.9	28.1	18.0	10.4	5.0	1.5
	ADTH 31	100	72.0	48.1	26.8	15.3	7.5	2.9
	ADTH 52	100	68.4	38.2	21.9	12.1	6.4	2.5
Floor conglomerates (*rudus*)	ADTH 3	100	29.5	15.9	9.4	5.6	3.0	1.3
	ADTH 15	100	37.5	23.1	11.6	5.7	3.1	1.1
	ADTH 25	100	43.4	28.2	15.8	6.9	3.9	1.3
	ADTH 32	100	34.6	22.3	15.8	10.6	5.7	2.4
	ADTH 33	100	42.6	29.5	19.2	11.2	7.0	3.1
Wall conglomerates (*trullisatio*)	ADTH 18	100	61.7	42.1	28.3	20.0	11.0	4.2
	ADTH 26	100	65.8	42.3	26.7	15.5	7.6	2.8
	ADTH 58	100	40.8	26.2	16.6	9.8	4.7	1.6
Vault concretes	ADTH 12	100	76.9	43.0	27.0	16.2	8.3	3.2
	ADTH 50	100	77.1	46.8	30.0	19.8	10.4	3.1
	ADTH 53	100	67.8	44.3	29.8	17.6	9.3	3.3
Plasters	ADTH 13	100	41.4	19.1	10.0	5.5	2.1	0.8
	ADTH 14	100	31.8	20.9	14.7	9.5	4.7	1.5

porous) on which to lay carefully the marble slabs in the floors or walls.

In regard to the water absorption, the imbibition coefficients (CI_W), closely related to weight He open porosity (Fig. 13a), highlight greater incidence of binder porosity (with coefficient correlation R^2 = 0.75; Fig. 13b, Table 10) with respect to the bulk mortar porosity (R^2 = 0.71; Fig. 13a, Table 9), including also the porosity created by aggregate immersed into the binder matrix. This is highlighted also by ADTH 26, ADTH 34, and ADTH 52 mortar samples which show high imbibition coefficients (37.0, 36.0, and 36.7 %, respectively; Table 9) and great He open porosity in the binder (50.3, 41.4, and 48.1 %, respectively; Table 10).

Saturation index (SI) of all mortar samples is always under the line of 100 % (Fig. 14) with average means ranging between 83.8 and 97.1 % (Table 9). Observing binder data, there is a higher variability of saturation index, ranging between 72.9 and 98.4 % (Table 10). This depends on high heterogeneity of binder matrix characterized by a variable open porosity (Table 10) and probably the complex geometry of porous carbonate network that affects the absorption and saturation processes. Some samples of binders are near or over the line of 100 % (Fig. 14), indicating the presence of hygroscopic minerals (e.g., phyllosilicates, etc.) as evidenced by XRD analysis on enriched binder samples.

Table 9 Physical properties of mortars (from Columbu et al. 2015b, modified)

Mortar typology	Sample	ρ_R (g/cm^3)	ρ_B (g/cm^3)	Φ_OHe (%)	$\Phi_O H_2O$ (%)	CI_W (%)	SI (%)	Is_{50} (MPa)
Brick bedding mortars	ADTH 4	2.66	1.36	48.82	42.91	31.32	87.90	0.35
	ADTH 6	2.65	1.42	46.21	38.33	26.80	82.95	0.11
	ADTH 11	2.71	1.49	45.13	41.73	27.94	92.46	0.14
	ADTH 21	2.40	1.35	43.82	40.12	28.49	91.55	0.15
	ADTH 35	2.43	1.51	37.70	37.00	24.36	98.15	0.25
	ADTH 42	2.61	1.57	39.83	35.65	22.61	89.51	0.55
	ADTH 43	2.48	1.49	39.96	37.65	25.19	94.21	0.28
	Mean	2.56	1.46	43.07	39.06	26.67	90.96	0.26
	SD	0.12	0.08	4.01	2.63	2.90	4.84	0.15
Cubilia bedding mortars	ADTH 23	2.69	1.36	49.59	41.86	30.63	84.41	0.77
	ADTH 46	2.70	1.51	44.12	36.79	24.20	83.37	0.32
	ADTH 54	2.50	1.47	41.02	39.53	26.56	96.35	0.37
	Mean	2.63	1.45	44.91	39.39	27.13	88.05	0.49
	SD	0.11	0.08	4.34	2.54	3.25	7.21	0.24
Floor-coating bedding mortars	ADTH 24	2.52	1.38	45.30	43.80	31.44	96.70	0.18
	ADTH 28	2.75	1.57	43.23	37.19	23.63	86.03	0.11
	ADTH 34	2.60	1.27	51.19	47.01	36.68	91.83	0.37
	ADTH 37	2.51	1.39	44.72	41.17	29.50	92.06	0.45
	Mean	2.60	1.40	46.11	42.29	30.31	91.66	0.28
	SD	0.11	0.12	3.50	4.16	5.39	4.37	0.16
Wall-coating bedding mortars	ADTH 7	2.64	1.40	47.17	37.53	26.71	79.56	0.08
	ADTH 31	2.68	1.49	44.48	37.41	25.04	84.12	0.37
	ADTH 52	2.61	1.25	51.98	45.56	35.99	87.64	0.31
	Mean	2.64	1.38	47.88	40.17	29.24	83.77	0.25
	SD	0.03	0.12	3.80	4.67	5.90	4.05	0.15
Floor conglomerates (*rudus*)	ADTH 3	2.67	1.56	41.37	40.14	25.48	97.04	0.95
	ADTH 15	2.59	1.49	42.70	36.73	24.63	86.02	0.47
	ADTH 25	2.48	1.40	43.57	39.56	26.96	90.78	0.57
	ADTH 32	2.54	1.47	41.99	36.72	24.80	87.44	0.41
	ADTH 33	2.65	1.57	40.98	36.36	23.11	88.73	0.26
	Mean	2.59	1.50	42.12	37.90	25.00	90.00	0.53
	SD	0.08	0.07	1.04	1.80	1.40	4.31	0.26
Wall conglomerates (*trullisatio*)	ADTH 18	2.62	1.35	48.43	39.06	28.66	80.64	0.11
	ADTH 26	2.25	1.21	46.38	44.94	36.96	96.89	0.57
	ADTH 58	2.21	1.46	34.14	32.81	22.31	96.08	0.47
	Mean	2.36	1.34	42.99	38.93	29.31	91.20	0.38
	SD	0.23	0.13	7.72	6.07	7.35	9.15	0.24
Vault concretes	ADTH 12	2.56	1.46	42.79	37.80	25.65	88.33	0.25
	ADTH 50	2.66	1.36	49.02	44.55	32.58	90.88	0.23
	ADTH 53	2.63	1.37	47.83	42.07	30.35	87.93	0.33
	Mean	2.62	1.40	46.55	41.47	29.53	89.05	0.27
	SD	0.05	0.06	3.30	3.41	3.54	1.60	0.05
Plasters (*arriccio*)	ADTH 13	2.44	1.55	36.64	36.19	23.28	98.79	0.64
	ADTH 14	2.54	1.53	39.64	37.82	24.59	95.40	0.71
	Mean	2.49	1.54	38.14	37.01	23.94	97.09	0.68
	SD	0.07	0.01	2.13	1.15	0.92	2.40	0.05

SD standard deviation, ρ_R real density, ρ_B bulk density, $\Phi_O He$ helium open porosity, $\Phi_O H_2O$ water open porosity, CI_W water imbibition coefficient, *SI* water saturation index, Is_{50} point load strength index

Table 10 Physical properties of binders and aggregate (from Columbu et al. 2015b, modified)

Binder and aggregate typology	Sample	ρ_R (g/cm^3)	ρ_B (g/cm^3)	Φ_OHe (%)	Φ_CHe (%)	Φ_T (%)	$\Phi_O H_2O$ (%)	CI_W (%)	SI (%)
Brick bedding mortar binders	ADTH 4	1.67	0.58	39.61	13.88	53.49	31.52	26.39	79.57
	ADTH 6	1.52	0.60	33.17	18.19	51.35	22.37	17.94	67.44
	ADTH 11	2.67	1.28	49.49	2.16	51.65	44.20	30.86	89.31
	ADTH 21	1.53	0.71	36.57	21.00	57.58	31.55	25.08	86.25
	ADTH 35	0.81	0.48	15.77	41.53	57.30	16.08	11.50	101.94
	ADTH 42	2.57	1.47	41.43	4.74	46.17	34.46	21.81	83.17
	ADTH 43	1.59	0.90	28.99	24.39	53.38	26.38	18.83	91.00
	Mean	1.77	0.86	35.00	17.99	52.99	29.51	21.77	85.53
	SD	0.65	0.38	10.68	13.21	3.90	9.03	6.37	10.66
Cubilia bedding mortar binders	ADTH 23	1.90	0.66	44.02	11.20	55.23	32.53	27.26	73.90
	ADTH 46	2.13	1.01	39.32	11.35	50.67	27.85	19.13	70.84
	ADTH 54	1.18	0.58	24.58	28.64	53.23	23.60	17.19	95.99
	Mean	1.74	0.75	35.97	17.07	53.04	28.00	21.19	80.24
	SD	0.50	0.23	10.14	10.03	2.28	4.47	5.34	13.72
Floor-coating bedding mortar binders	ADTH 24	1.44	0.59	34.25	19.95	54.20	33.24	26.80	97.07
	ADTH 28	1.42	0.60	27.40	20.79	48.19	20.01	12.73	73.05
	ADTH 34	1.47	0.38	41.37	12.17	53.54	36.32	33.53	87.78
	ADTH 37	2.43	1.16	51.14	6.32	57.46	45.48	35.48	88.95
	Mean	1.69	0.68	38.54	14.81	53.35	33.77	27.13	86.71
	SD	0.49	0.34	10.15	6.86	3.84	10.54	10.30	10.00
Wall-coating bedding mortar binders	ADTH 7	1.90	0.74	42.37	12.62	54.98	27.38	22.16	64.61
	ADTH 31	2.36	1.13	44.19	7.50	51.69	32.50	22.96	73.54
	ADTH 52	1.76	0.48	48.10	10.12	58.22	38.76	36.16	80.59
	Mean	2.01	0.78	44.89	10.08	54.97	32.88	27.09	72.91
	SD	0.31	0.33	2.93	2.56	3.26	5.70	7.86	8.01
Floor conglomerate (*rudus*) binders	ADTH 3	1.49	0.77	25.88	23.93	49.81	25.66	16.26	99.13
	ADTH 15	1.90	0.95	36.03	16.19	52.22	27.42	19.63	76.11
	ADTH 25	1.23	0.50	30.86	22.69	53.55	26.43	19.71	85.64
	ADTH 32	1.53	0.74	31.34	22.20	53.53	24.65	18.24	78.66
	ADTH 33	1.71	0.89	30.06	20.12	50.18	24.32	15.56	80.90
	Mean	1.57	0.77	30.83	21.03	51.86	25.69	17.88	84.09
	SD	0.25	0.17	3.62	3.03	1.79	1.27	1.91	9.11
Wall conglomerate (*trullisatio*) binders	ADTH 18	1.83	0.60	46.09	11.53	57.62	32.23	27.23	69.92
	ADTH 26	1.64	0.63	50.31	15.79	66.10	49.47	47.19	98.34
	ADTH 58	0.92	0.68	16.63	49.72	66.35	16.19	12.62	97.33
	Mean	1.46	0.64	37.68	25.68	63.36	32.63	29.01	88.53
	SD	0.48	0.04	18.35	20.92	4.97	16.65	17.35	16.12
Vault concrete binders	ADTH 12	1.54	0.75	30.80	21.87	52.67	24.09	17.90	78.22
	ADTH 50	1.38	0.41	35.04	14.93	49.97	29.68	25.12	84.69
	ADTH 53	1.58	0.57	37.08	15.77	52.86	29.32	24.24	79.07
	Mean	1.50	0.57	34.31	17.52	51.83	27.70	22.42	80.66
	SD	0.10	0.17	3.21	3.79	1.62	3.13	3.94	3.52
Plasters (*arriccio*) binders	ADTH 13	2.58	1.61	41.49	5.00	46.49	42.08	27.53	101.40
	ADTH 14	1.58	0.87	28.60	23.90	52.49	27.31	18.28	95.50
	Mean	2.08	1.24	35.05	14.45	49.49	34.69	22.91	98.45
	SD	0.70	0.52	9.12	13.36	4.24	10.44	6.55	4.17
Volcanic scoria aggregates	ADTH 33 b	2.40	1.46	39.28	n.d.	n.d.	38.01	26.07	96.90
	ADTH 18 b	2.53	1.53	39.74	n.d.	n.d.	39.07	25.63	98.44

Table 10 (continued)

Binder and aggregate typology	Sample	ρ_R (g/cm^3)	ρ_B (g/cm^3)	Φ_OHe (%)	Φ_CHe (%)	Φ_T (%)	$\Phi_O H_2O$ (%)	CI_W (%)	SI (%)
	ADTH 50 b	2.56	1.57	38.54	n.d.	n.d.	37.93	24.18	98.55
	ADTH 11 b	2.58	1.67	35.42	n.d.	n.d.	35.20	21.13	99.55
	ADTH 34 b	2.56	1.63	36.27	n.d.	n.d.	36.15	22.16	99.81
	ADTH 14 b	2.53	1.61	36.26	n.d.	n.d.	36.21	22.47	100.01
	ADTH 12 b	2.51	1.55	38.21	n.d.	n.d.	32.46	20.69	84.96
	Mean	2.53	1.57	37.67	n.d.	n.d.	36.43	23.19	96.89
	SD	0.06	0.07	1.68	n.d.	n.d.	2.20	2.13	5.37
Leucitite aggregates	ADTH 35 l	2.87	2.16	24.68	n.d.	n.d.	23.66	10.94	95.89
	ADTH 58 l	2.88	2.06	28.52	n.d.	n.d.	26.11	12.66	91.57
	ADTH 25 l	2.87	2.18	25.68	n.d.	n.d.	20.87	9.56	87.48
	Mean	2.87	2.13	26.29	n.d.	n.d.	23.55	11.05	91.65
	SD	0.01	0.06	1.99	n.d.	n.d.	2.62	1.55	4.21
Cocciopesto aggregates	ADTH 18 c	2.85	1.58	44.49	n.d.	n.d.	38.39	24.11	86.30
	ADTH 25 c	2.30	1.92	16.61	n.d.	n.d.	12.27	7.49	73.86
	ADTH 3 c	2.92	1.52	47.97	n.d.	n.d.	42.52	27.82	88.65
	ADTH 11 c	1.95	1.68	13.67	n.d.	n.d.	13.44	7.02	98.29
	Mean	2.51	1.68	30.68	n.d.	n.d.	26.65	16.61	86.78
	SD	0.46	0.17	18.04	n.d.	n.d.	16.03	10.91	10.05

The physical properties were calculated in a theoretical way using the physical properties of the mortars and composition percentages of aggregates determined by modal analysis (Table ESM2), according to the following general formula: X_n (B) = [X_n (M) − ($X_{n\,(a)} \times \%_{(a)}$) − ($X_{n\,(b)} \times \%_{(b)}$) − ($X_{n\,(c)} \times \%_{(c)}$) − ($X_{n\,(d)} \times \%_{(d)}$) − ($X_{n\,(e)} \times \%_{(e)}$) − ($X_{n\,(f)} \times \%_{(f)}$)]/% (A)

SD standard deviation; *X* physical properties; *(M)* mortar; *(B)* binder; *(A)* aggregate; *n* number from 1 to 6 of different physical properties, with X_1 = real density, X_2 = bulk density, X_3 = He open porosity, X_4 = H_2O open porosity, X_5 = He closed porosity, and X_6 = imbibition coefficient; ρ_R real density; ρ_B bulk density; $\Phi_O He$ helium open porosity; $\Phi_C He$ helium closed porosity; Φ_T total porosity; $\Phi_O H_2O$ water open porosity; CI_W water imbibition coefficient; *SI* water saturation index; *(a)* scoria; *(b)* leucitite; *(c) cocciopesto*; *(d)* marble; *(e)* clinopyroxene; *(e)* green hornblende; *(f)* biotite. The saturation index of binders is calculated as SI = ($\Phi_O H_2O/\Phi_O He$) × 100. The solid density of binder is assumed to be 2.80 g/cm^3 as average of literature data. *SD* standard deviation, *n.d.* not determined

The volcanic aggregates (leucitic basalt and leucitites) show a saturation index close to 100 % (Fig. 14), while the aggregates and *lateritious* fragments (bricks, tiles, and crushed pottery) show lower average values of saturation index (Fig. 14, Table 10), probably due to a lower radius of porosity (or greater tortuosity) with respect to the binder matrix and the bulk mortar samples.

To observe the physical-hydraulic behavior of bulk mortars, the water absorption kinetic (Table 11) is reported in Fig. 15.

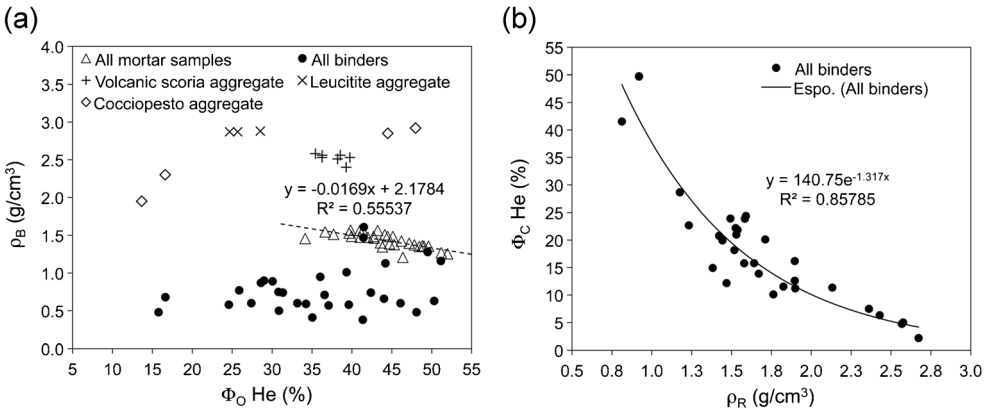

Fig. 12 Physical properties of mortars, binders, and aggregates: **a** helium open porosity (Φ_OHe) versus bulk density (ρ_B); **b** real density (ρ_R) versus helium closed porosity (Φ_OHe)

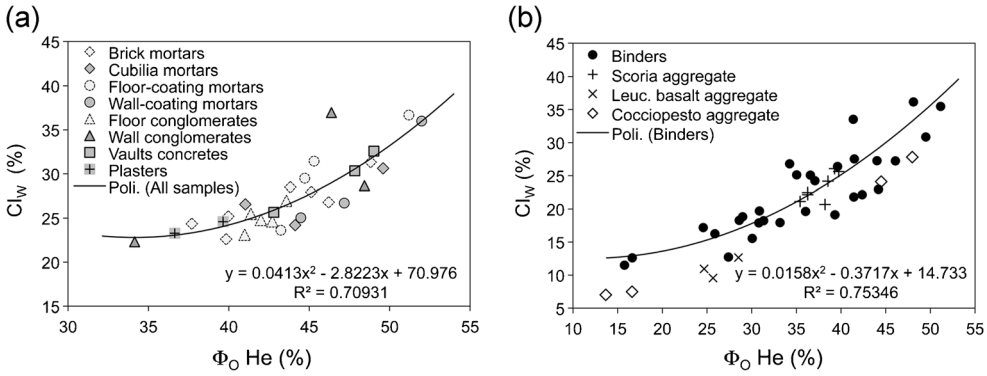

Fig. 13 Physical properties of mortars, binders, and aggregates: **a** helium open porosity (Φ_OHe) versus imbibition coefficient (CI_W) of mortars; **b** helium open porosity (Φ_OHe) versus imbibition coefficient (CI_W) of binders and aggregates

Strength index and hydraulic degree of mortars

The physical mechanical characteristics (Table 12) of mortars and aggregate are shown in Fig. 16a, where the punching strength index (Is_{50}) versus He open porosity reported is normally well negatively correlated.

The low punching index (with value <1 MPa) and the very low correlation ($R^2 = 0.20$) with helium open porosity indicate that the resistance of mortars is affected by different factors: (1) the porosity of bulk mortar sample, (2) small dimensions of the specimens with respect to aggregate size, and (3) characteristics of the binder (i.e., cohesion degree, porosity, etc.). However, it is possible to make some evaluations. Except for the plasters, the floor conglomerates and bedding mortars show greater mechanical resistances (0.53 ± 0.26 MPa and 0.49 ± 0.24 MPa, respectively; Tables 9 and 12) with respect to other mortars (ranging between 0.25 and 0.28 MPa), probably due to a presence of an aggregate with high quality, as evidenced by physical data of samples ADTH 25C and ADTH 11C (Table 10) and those of the *lateritious* samples from *Heliocaminus* Baths and "Grandi Terme" Baths (Columbu et al. 2015b). The higher resistance of the plasters with respect to other mortars can be explained by lower helium open porosity (38.14 ± 2.13 %; Table 9) and higher bulk density (1.54 ± 0.01 g/cm^3), probably due to better mixing of binder-aggregate and pressing of *arriccio* layer.

The diagram of Fig. 16b, which reports strength index versus CO_2/H_2O for all mortars and lime-lumps (generally inversely correlated with hydraulic degree), highlights a negative correlation between the hydraulic degree and mechanical resistance, as better evidenced by correlation coefficient ($R^2 = 0.57$) of Fig. 16c, in which the mortars with medium-coarse aggregate were excluded (i.e., vault concretes, floor, and wall conglomerates).

Overall, the physical-mechanical tests show that the strength of mortars depends on (1) porosity of bulk mortar sample, represented by discontinuities between aggregate and binder and porous binder matrix; (2) hydraulic degree of mortar; and (3) sorting degree and particle size of the aggregate (see samples ADTH 4, 42, 54, from bedding mortars of brick and *cubilia*, characterized by higher sorting with modal class between 2000 and 1000 μm than other mortars with modal class of 4000 μm). Subordinately, the mechanical resistance depends on (1) dimensional relationship between aggregate and specimen, and (2) thickness of mortar, as evidenced by low values in the vault concretes and high strengths in the *arriccio* plasters.

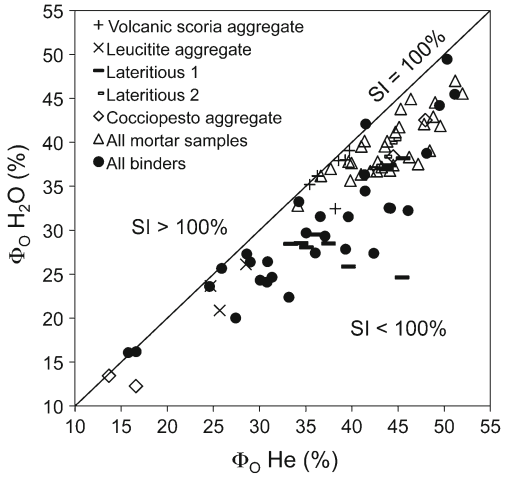

Fig. 14 Physical properties of mortars, binders and aggregates: helium open porosity (Φ_OHe) versus water open porosity ($\Phi_O H_2O$), reporting the line of saturation index at 100 %

Conclusions

The results highlight that the construction of the *Heliocaminus* baths respects the general architectural and structural issues of the Roman period. This ancient building was mainly constructed using bricks and volcanic stones (i.e., *cubilia* for

Table 11 Kinetic water-absorption curves determined for total immersion on cubic bulk specimens (weight measurements every 24 h)

Mortar typology	Sample	Water absorption (%)									
		24 h	48 h	72 h	96 h	120 h	144 h	168 h	192 h	216 h	240 h
Brick bedding mortars	ADTH 4	28.53	29.44	29.91	30.53	30.86	30.94	31.10	31.28	31.31	31.32
	ADTH 6	23.16	24.20	24.99	25.44	25.94	26.11	26.26	26.46	26.69	26.80
	ADTH 11	24.97	25.53	26.03	26.74	27.24	27.33	27.55	27.49	27.95	27.94
	ADTH 21	25.44	25.87	26.30	26.71	27.00	27.32	27.62	27.92	28.49	28.49
	ADTH 35	22.79	23.26	23.34	23.88	24.25	24.29	24.15	24.07	24.36	24.36
	ADTH 42	19.53	20.38	21.21	21.77	22.03	22.46	22.61	22.35	22.61	22.61
	ADTH 43	22.17	23.03	23.39	24.21	24.15	24.47	24.84	24.77	25.19	25.19
Cubilia bedding mortars	ADTH 23	27.86	27.95	28.08	28.78	29.14	29.70	29.96	30.03	30.35	30.63
	ADTH 46	21.86	22.40	22.59	22.86	23.04	23.18	23.31	23.68	24.20	24.20
	ADTH 54	24.45	23.70	23.92	25.22	25.41	25.00	25.44	25.64	26.56	26.56
Floor-coating bedding mortars	ADTH 24	27.43	27.95	28.32	29.01	29.55	30.24	30.57	30.75	31.44	31.44
	ADTH 28	21.44	21.97	22.13	22.35	22.46	22.75	22.95	23.11	23.63	23.63
	ADTH 34	32.28	32.89	33.61	33.78	34.39	34.65	35.08	35.54	36.68	36.68
	ADTH 37	26.75	27.14	27.67	28.27	28.38	28.50	28.54	28.52	29.50	29.50
Wall-coating bedding mortars	ADTH 7	24.93	24.97	25.09	25.41	25.73	25.91	26.31	26.51	26.71	26.71
	ADTH 31	23.83	23.99	24.06	24.25	24.46	24.65	24.86	24.95	25.02	25.04
	ADTH 52	31.49	33.03	33.39	33.87	34.45	34.58	34.69	35.04	35.99	35.99
Floor conglomerates (*rudus*)	ADTH 3	22.78	23.67	24.16	24.31	24.47	24.87	25.05	24.88	25.48	25.48
	ADTH 15	23.40	23.47	23.51	23.71	23.90	24.10	23.31	24.51	24.63	24.63
	ADTH 25	24.14	25.21	26.23	26.53	26.72	26.86	26.93	26.96	26.96	26.96
	ADTH 32	20.33	21.04	22.20	23.19	23.32	23.69	23.98	24.34	24.80	24.80
	ADTH 33	19.24	19.93	20.09	21.05	21.51	21.95	22.23	22.60	23.11	23.11
Wall conglomerates (*trullisatio*)	ADTH 18	24.35	26.37	26.56	27.33	27.44	27.76	27.80	28.05	28.66	28.66
	ADTH 26	34.47	35.18	35.38	35.32	35.59	35.63	35.96	36.08	36.96	36.96
	ADTH 58	20.66	20.48	20.69	21.20	21.14	21.60	21.66	21.52	22.31	22.31
Vault concretes	ADTH 12	22.73	23.22	23.76	24.20	24.20	24.75	25.23	25.01	25.65	25.65
	ADTH 50	28.37	29.18	29.98	30.98	31.83	31.67	31.70	31.91	32.58	32.58
	ADTH 53	26.21	26.69	27.16	27.94	28.41	28.77	29.32	29.81	30.35	30.35
Plasters	ADTH 13	21.19	21.75	22.17	22.38	22.64	22.71	22.83	22.92	23.29	23.28
	ADTH 14	22.15	22.79	23.17	23.83	24.00	24.03	24.08	24.14	24.59	24.59

ashlars) outcropping within the area of Hadrian's Villa, and hydraulic mortars.

Volcanic rocks, *cocciopesto*, and crystal-clasts were used as aggregate of mortars. Volcanics mainly consist of red and black leucitic basaltic scoria and subordinately leucitites belonging to the alkaline rocks of ultrapotassic series of the Roman Magmatic Province, outcropping around the area of Hadrian's Villa. The basaltic scoria aggregate reacts with binder while the leucitite does not show reactivity, probably due to high crystallinity and near absence of glass in the matrix.

In the conglomerates (*trullisatio* and *rudus*) and plasters (*arriccio*), the *cocciopesto* was also used, with medium-coarse particle size (frequency range 6–30 mm), while in the floor marble-coating mortars, a *cocciopesto* aggregate with smaller size (<8 mm) was used. As evidenced by different physical properties, the *cocciopesto* shows different quality, as a function of the kind and quality of ceramic material crushed (e.g., bricks, pottery, tiles). In any case, as shown by reaction borders with the binder, the *cocciopesto* aggregate gives good pozzolanic characteristics to the mortars.

The diffraction (XRPD) and thermal (TG/DSC) analyses on the fractions enriched in binder highlight the main presence of calcite. Quartz, leucite, and mica (i.e., muscovite) are also present as residual phases of aggregate. Owing to the pozzolanic reactions, the hydraulic phases of new formation have not been

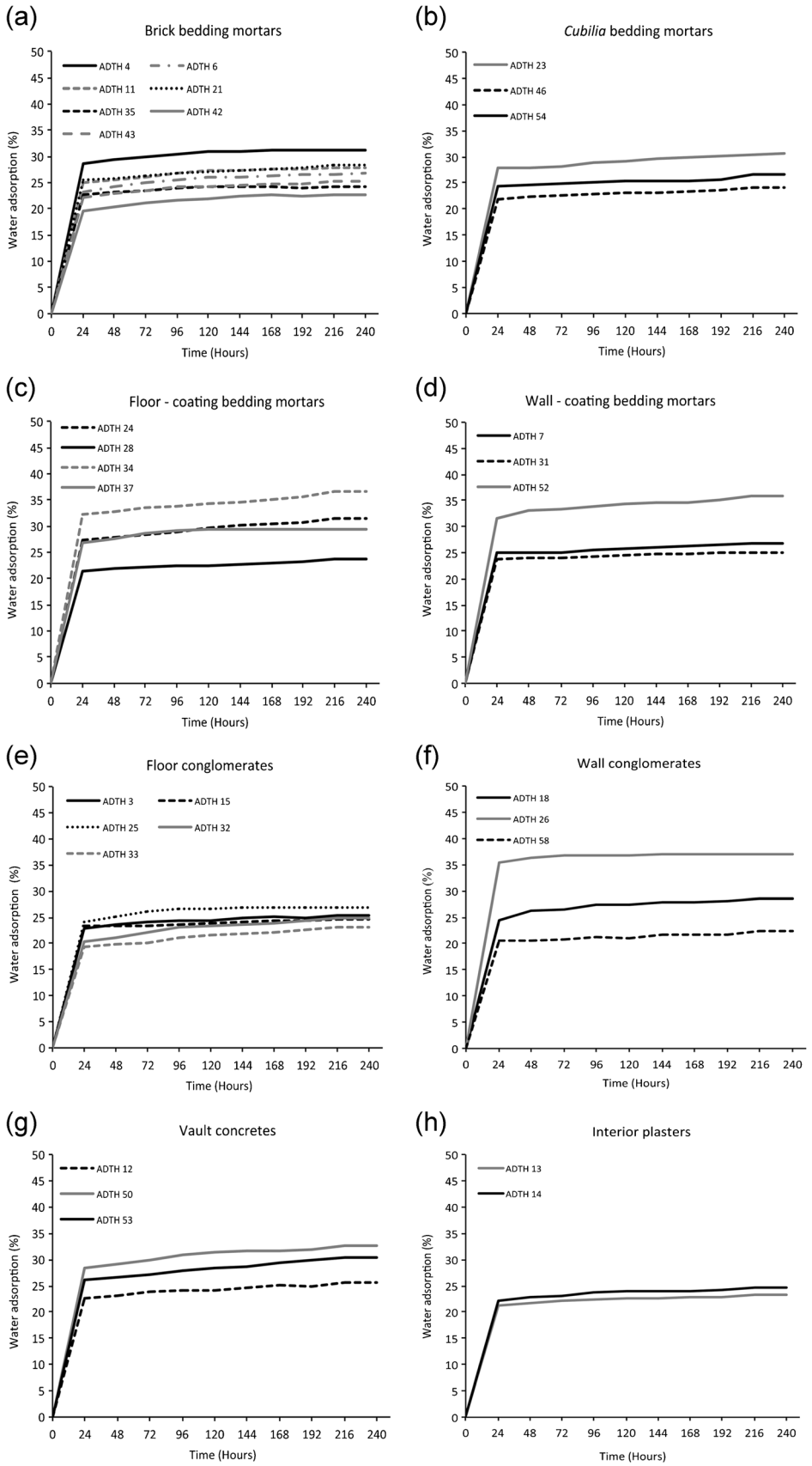

Fig. 15 Physical properties of mortars: absorption kinetics for each mortar group, where time (h) versus water absorption (progressive CI_W) is reported

Table 12 Data of point load test for the determination of punching strength index (Is_{50}) on cubic bulk specimens of mortars

Mortar typology	Sample	D (mm)	W (mm)	$2L$ (mm)	P (N)	$A = WD$ (mm^2)	D_e^2 (mm^2)	D_e (mm)	Is_{50} (MPa)	R_C (MPa)	R_T (MPa)
Brick bedding mortars	ADTH 4	13.50	16.50	10.6	160	222.75	283.62	16.84	0.35	4.84	0.43
	ADTH 6	14.00	16.00	11.0	50	224.00	285.21	16.89	0.11	1.51	0.13
	ADTH 11	14.00	15.00	10.25	60	210.00	267.39	16.35	0.14	1.90	0.17
	ADTH 21	9.20	15.50	10.5	50	142.60	181.57	13.47	0.15	2.14	0.19
	ADTH 35	14.10	16.90	10.5	120	238.29	303.41	17.42	0.25	3.45	0.31
	ADTH 42	15.30	16.50	10.75	280	252.45	321.44	17.93	0.55	7.69	0.69
	ADTH 43	16.10	17.10	10.35	150	275.31	350.55	18.72	0.28	3.85	0.34
Cubilia bedding mortars	ADTH 23	13.40	14.00	10.5	310	187.60	238.87	15.46	0.77	10.71	0.96
	ADTH 46	13.80	16.10	11.5	150	222.18	282.90	16.82	0.32	4.55	0.41
	ADTH 54	14.30	14.30	9.55	160	204.49	260.37	16.14	0.37	5.17	0.46
Floor-coating bedding mortars	ADTH 24	12.00	17.40	10.5	80	208.80	265.86	16.31	0.18	2.54	0.23
	ADTH 28	15.90	16.50	10.45	60	262.35	334.04	18.28	0.11	1.60	0.14
	ADTH 34	12.80	16.20	10.75	160	207.36	264.03	16.25	0.37	5.12	0.46
	ADTH 37	14.10	16.10	9.5	210	227.01	289.05	17.00	0.45	6.26	0.56
Wall-coating mortars	ADTH 7	15.00	15.50	10.25	40	232.50	296.04	17.21	0.08	1.17	0.10
	ADTH 31	13.40	14.00	10.5	150	187.60	238.87	15.46	0.37	5.18	0.46
	ADTH 52	13.50	16.00	11.15	140	216.00	275.03	16.58	0.31	4.34	0.39
Floor conglomerates (*rudus*)	ADTH 3	14.00	15.90	9.5	440	222.60	283.43	16.84	0.95	13.32	1.19
	ADTH 15	13.80	16.20	10.05	220	223.56	284.65	16.87	0.47	6.64	0.59
	ADTH 25	12.50	17.50	10.75	260	218.75	278.53	16.69	0.57	7.98	0.71
	ADTH 32	14.90	15.00	10.5	190	223.50	284.58	16.87	0.41	5.73	0.51
	ADTH 33	15.50	11.60	10.4	100	179.80	228.94	15.13	0.26	3.57	0.32
Wall conglomerates (*trullisatio*)	ADTH 18	14.10	16.20	9.75	50	228.42	290.84	17.05	0.11	1.48	0.13
	ADTH 26	14.40	17.50	10.5	290	252.00	320.87	17.91	0.57	7.97	0.71
	ADTH 58	14.10	16.10	10.95	220	227.01	289.05	17.00	0.47	6.56	0.59
Vault concretes	ADTH 12	13.40	15.80	9.5	110	211.72	269.58	16.42	0.25	3.46	0.31
	ADTH 50	12.00	17.20	10.5	100	206.40	262.80	16.21	0.23	3.21	0.29
	ADTH 53	13.90	15.70	10.45	150	218.23	277.87	16.67	0.33	4.61	0.41
Plasters	ADTH 13	16.50	16.70	13.0	350	275.55	350.85	18.73	0.64	8.98	0.80
	ADTH 14	16.20	17.10	10.0	390	277.02	352.72	18.78	0.71	9.96	0.89

Distance between two punches (higher of specimen); W specimen width, $2L$ specimen length, P rupture load, $A = WD$ section of rupture of the specimen, D_e equivalent diameter, Is_{50} PLT strength index, R_C theoretical compression strength, R_T theoretical tensile strength (according to ISRM, International Society For Rock Mechanics, 1985)

identified by x-ray diffraction due to their small amount and, therefore, because these are probably amorphous phases (gel-like C-S-A-H).

Gypsum and ettringite are sporadically present, indicating an advanced alteration degree. The first is due to sulfation processes, facilitated by the high open porosity calculated on the binder matrix. Ettringite is formed as a consequence of the chemical reaction between the sulfates and aluminates which are present in the hydration products.

The use and mixing of aggregate and binder in the production of mortar are made according to the Roman standard methods known at the time, with different mixtures and hydraulic degree in relation to the function in the masonry as well as suggested by *Vitruvio*.

Nevertheless, the physical-mechanical analysis show low values of punching strength index with respect to the standards of other Roman mortars. The low values depend mainly on high porosity of bulk mortar due to an evident chemical-physical decay by (1) dissolution of the binder and (2) hydration/dehydration/crystallization of gypsum, ettringite, etc. that involves a high increment of volume with mortar disintegration (cracking and loss of mass). Except for the *cocciopesto* conglomerates, the low mechanical resistance can also be due to an imperfect production and laying of mortars or incomplete mixing of aggregate with binder. Despite the low values, using CO_2/H_2O ratio data of TG/DSC analysis, a positive correlation (R^2 = 0.57) between hydraulic

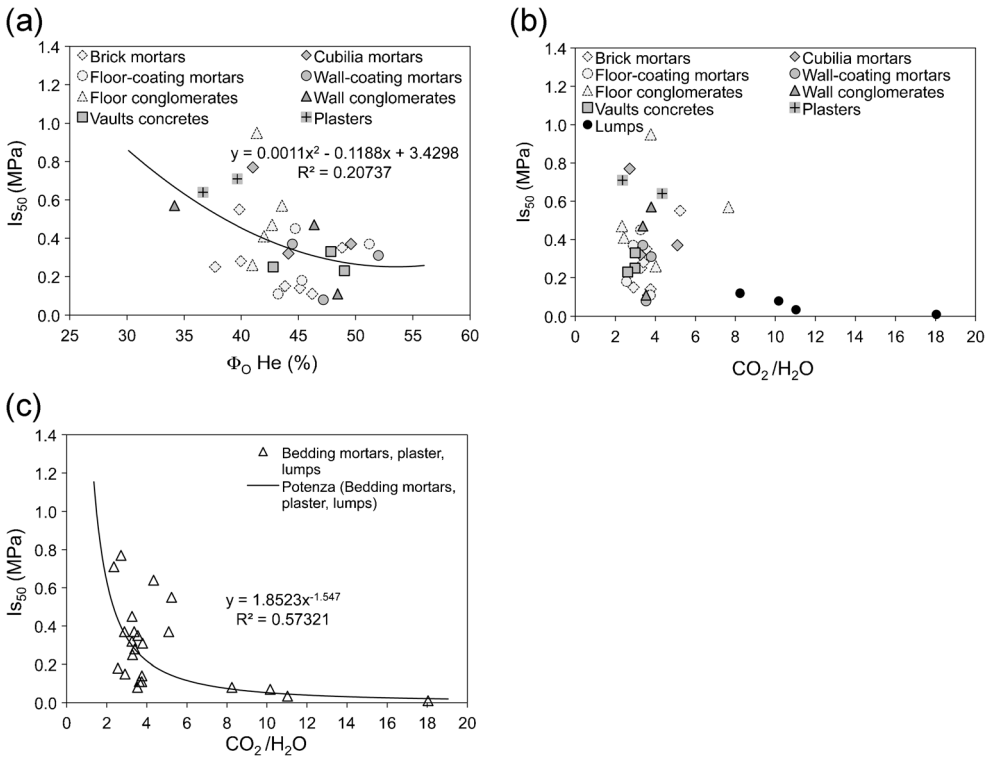

Fig. 16 Physical properties of mortars, binders, and aggregates: **a** helium open porosity (Φ_OHe) versus point load strength index (Is_{50}) of all mortars; **b** CO_2/H_2O versus point load strength index (Is_{50}) of all mortars and lumps; **c** CO_2/H_2O versus point load strength index (Is_{50}) of bedding mortars and lumps

degree and mechanical strength was found, showing the important function of pozzolanic aggregate in the mortars.

The high variability of some physical properties (bulk density, porosity, particle size of aggregate) in some cases within groups of samples, together with the short time of bath construction, show that the production and processing of the mortars were made quickly, probably also in discontinuous ways with changes of the workforce.

The latter allows us to imagine that that there may have been many small construction phases. Then, considering that the complex represents an "experimental building" to test new solutions in re-invention of architectonic spaces, several construction phases can be related to rethinking during the design and organization of various spaces or the functionality of the baths (e.g., heating system, where the furnaces beneath the *sudatio* room have never been used for significant periods).

These construction evidences were highlighted by an accurate digital survey (Columbu et al. 2015b) that supports the theory of a building of new conception, with advanced technical solutions, in some cases with poor results, with numerous changes in technical and building solutions.

Acknowledgments Thanks to Dr. Benedetta Adembri of the "Soprintendenza per i Beni Archeologici del Lazio" for the support and collaboration, and Giorgio Verdiani, Dipartimento di Architettura of Florence University (UNIFI), Italy, responsible for the operative group of digital survey.

References

Adam JP (2006) L'arte di costruire presso i romani, materiali e tecniche vol 10. Longanesi

Adriano P, Santos Silva A, Veiga R, Mirão J, Candeias AE (2009) Microscopic characterization of old mortars from Santa Maria Church in Énvora. Material Characterization 60(7):610–620

Antonelli F, Columbu S, Lezzerini M, Miriello D (2013) Petrographic characterization and provenance determination of the white marbles used in the Roman sculptures of Forum Sempronii (Fossombrone, Marche, Italy). Applied Physics A 115:1033–1040

Antonelli F, Columbu S, De Vos Raaijmakers M, Andreoli M (2014) An archaeometric contribution to the study of ancient millstones from the Mulargia area (Sardinia, Italy) through new analytical data on volcanic raw material and archaeological items from Hellenistic and Roman North Africa. J Archaeol Sci 50:243–261

Attanasio D, Mesolella G, Pensabene P, Platania R, Rocchi P (2009) EPR and petrographic provenance of the architectural white marbles of three buildings at Villa Adriana. In: Maniatis Y (Ed.), Asmosia VII. Proceeding 7th International Conference ASMOSIA, Thassos 2003, Bulletin de Correspondance Hellenique Sup., 51, Athens, pp. 57–369

Attanasio D, Bruno M, Prochaska W, Yavuz AB (2013) The Asiatic marbles of the Hadrian's Villa at Tivoli. J Archaeol Sci 40: 4358–4368

Babini C, Fiori C (1996) Impiego delle analisi termiche nello studio delle malte, stucchi, intonaci e finiture murarie, Mosaico-analisi dei materiali e problematiche del restauro parte 2. CNR-Consiglio Nazionale Delle Ricerche, Ravenna

Bakolas A, Biscontin G, Contardi V, Franceschi E, Moropoulou A, Palazzi D, Zendri E (1995) Thermoanalytical research on traditional mortars in venice. Thermochimica Acta 269-270:817–828

Bakolas A, Biscontin G, Moropoulou A, Zendri E (1998) Characterization of structural byzantine mortars by thermogravimetric analysis. Termochimica Acta volume 321 1(2):151–160

Bertorino G, Franceschelli M, Marchi M, Luglié C, Columbu S (2002) Petrographic characterisation of polished stone axes from Neolithic Sardinia, archaeological implications. Per Mineral, Special Issue: Archaeometry and Cultural Heritage 71:87–100

Branda F, Luciani G, Costantini A, Piccioli C (2001) Interpretation of the Thermogravimetric Curves of Ancient Pozzolanic Concretes. Archaeometry 43(4):447–453

Bultrini G, Fragala I, Ingo GM, Lanza G (2006) Minero-petrographic, thermal and microchemical investigation of historical mortars used in Catania (Sicily) during the XVII century a.D. Applied Physics A 83(4):529–536

Cagnana A (2000) Archeologia dei materiali da costruzione. SAP Società Archeologica S.r.l., Mantova

Cicerchia P (1985) Sul carattere distributivo delle terme con *Heliocaminus* di Villa Adriana. Xenia 9:47–60

Callebaut K, Elsen J, Van Balen K, Viaene W (2001) Nineteenth century hydraulic restoration mortars in the Saint Michael's Church (Leuven, Belgium). Cement and Concrete Research 31(3):397–403

Columbu S, Verdiani G (2011) From the small elements to the urban scale: an investigation where petrophysical study of materials and architectural shape analysis try to read a masterplan in the Hadrian's Villa, Tivoli (Rome, Italy). In: Proceedings of 16th International Conference on Cultural Heritage and New Technologies (CHNT 2011) Wien. 14–16 November 2011, Urban Archaeology and Prospection, Museen der Stadt Wien–Stadtarchäologie. eBook Ed., vol. 1, part 3, pp. 273–293

Columbu S, Garau AM, Macciotta G, Marchi M, Marini C, Carboni D, Ginesu S, Corazza G (2011) Manuale sui materiali lapidei vulcanici della Sardegna centrale e dei loro principali impieghi nel costruito. Iskra Edizioni, Ghilarza (OR), p. 302

Columbu S, Verdiani G (2012) From the small elements to the urban scale: an investigation where petrophysical study of materials and architectural shape analysis try to read a masterplan in the Hadrian's Villa, Tivoli (Rome, Italy). In: Börner W, Uhlirz S (Eds), Proceedings of 16th International Conference on Cultural Heritage and New Technologies 2011 (CHNT16), Wien. Museen der Stadt Wien–Stadtarchäologie Ed., vol. 1, part 3, pp. 273–293

Columbu S, Guccini G (2013) Decay processes and three-dimensional digital modelling for geometric-spatial reconstruction of the volcanic stone called "the elephant" of Neolithic "domus de janas" (Sardinia, Italy): investigation and preliminary data. In: Börner, W., Uhlirz, S. (Eds.), Proceedings of the 17th International Conference on Cultural Heritage and New Technologies 2012 (CHNT 17), Wien. Museen der Stadt Wien–Stadtarchäologie Ed., vol. 1, part 3, pp. 1–21

Columbu S, Guccini G, Verdiani G (2013) Petro-physical characterization and 3D digital modeling for geometric reconstruction of the Neolithic "domus de janas" of Sedini field (North-Sardinia, Italy. Advances in Computer Science: An International Journal 1:70–80

Columbu S, Verdiani G (2014) Digital survey and material analysis strategies for documenting, monitoring and study the Romanesque churches in Sardinia, Italy. Lecture Notes in Computer Science, Springer 8740:446–453

Columbu S, Antonelli F, Lezzerini M, Miriello D, Adembri B, Blanco A (2014a) Provenance of marbles used in the *Heliocaminus* Baths of Hadrian's Villa (Tivoli, Italy. J Archaeol Sci 49:332–342

Columbu S, Gioncada A, Lezzerini M, Marchi M (2014b) Hydric dilatation of ignimbritic stones used in the church of Santa Maria di Otti (Oschiri, northern Sardinia, Italy. Ital J Geosci 133:149–160

Columbu S, Marchi M, Carcangiu T (2014c) Le vulcaniti mioceniche sarde utilizzate come materiali costruttivi nell'architettura storica: l'esempio della chiesa Romanica di San Pietro di Zuri (Sardegna, Italia). In: Martorelli R (ed), "Itinerando" dalla preistoria ad oggi. Morlacchi Editore, Perugia, Vol. 1.1, pp 727–744

Columbu S, Cruciani G, Fancello D, Franceschelli M, Musumeci M (2015a) Petrophysical properties of a granite-protomylonite-ultramylonite sequence: insight from the Monte Grighini shear zone, central Sardinia, Italy. European Journal of Mineralogy 27, 4:471–486

Columbu S, Sitzia F, Verdiani G (2015b) Contribution of petrophysical analysis and 3D digital survey in the archaeometric investigations of the Emperor Hadrian's Baths (Tivoli, Italy). Rendiconti Lincei 26,4: 455–474

Columbu S, Marchi M, Martorelli R, Palomba M, Pinna F, Sitzia F, Tanzini L, Virdis A (2015c) Romanesque and Territory. The construction materials of Sardinian Medieval churches: new approaches to the valorisation, conservation and restoration. In: Börner, W., Uhlirz, S. (Eds.), Proceedings of 16th International Conference on Cultural Heritage and New Technologies 2011 (CHNT16), Wien. Museen der Stadt Wien–Stadtarchäologie Ed., vol. 1, part 3, pp. 1–15

Coroneo R, Columbu S (2010) Sant'Antioco di Bisarcio (Ozieri): La cattedrale romanica e i materiali costruttivi. Archeoarte 1:145–173

Crisci GM, De Francesco AM, Gagliardi F, Mercurio P, Miriello D (2001) L'analisi composizionale delle malte: metodo di studio delle fasi costruttive in architettura. Arkos 4:34–41

Crisci GM, De Francesco AM, Gagliardi F, Mercurio P, Gattuso C, Miriello D. (2002) L'analisi composizionale delle malte: Un valido mezzo per risalire alle fasi costruttive. Risultati preliminari. In Proceedings of II Congresso nazionale di archeometria, pp 485–494

De Luca R, Cau Ontiveros MA, Miriello D, Pecci A, Le Pera E, Bloise A, Crisci GM (2013) Archaeometric study of mortars and plasters from the Roman City of Pollentia (Mallorca-Balearic Islands). Per. Mineral. 82:353–379

Drdácky M, Fratini F, Frankeová D, Slízˇková Z (2013) The Roman mortars used in the construction of the Ponte di Augusto (Narni, Italy). A comprehensive assessment. Constr Build Mater 38:1117–1128

Giuliani Cairoli F (2006) L'edilizia nell'antichità. Carocci, Roma

ISRM International Society For Rock Mechanics (1972) Suggest method for determining the point load strength index. ISRM (Lisbon, Portugal). Committee on field tests. Document n.1, pp. 8–12

ISRM, International Society For Rock Mechanics (1985) Suggest method for determining the point load strength. ISRM commission for testing methods, Working group on revision of the point load

Lapuente P, León P, Nogales T, Royo H, Preite-Martinez M, Blanc Ph (2012) White sculptural materials from Villa Adriana: study of provenance. In: Gutiérrez Garcia A, Lapuente P, Rodà I (Eds.), Interdisciplinary studies on Ancient Stone. Proceedings of the IX ASMOSIA Conference, Tarragona, pp. 364–375

Lezzerini M, Antonelli F, Columbu S, Gadducci R, Marradi A, Miriello D, Parodi L, Secchiari L, Lazzeri A (2016) The documentation and conservation of the cultural heritage: 3D laser scanning and GIS techniques for thematic mapping of the stonework of the Façade of St. Nicholas Church (Pisa, Italy). International Journal of Architectural Heritage: Conservation, Analysis, and Restoration 10(1):9–19

Mac Donald WL, Pinto JA (2006) Villa Adriana: la costruzione e il mito da Adriano a Louis I. Kahn. Electa Architettura Paperback, Milano

Macciotta G, Bertorino G, Caredda A, Columbu S, Coroneo R, Franceschelli M, Marchi M, Rescic S (2001) The S.Antioco of Bisarcio Basilica (NE Sardinia, Italy): water-rock interaction in ignimbrite monument decay. Water-Rock Interaction (WRI-10), Cidu Ed, Swets and Zeitlinger, Lisse 1:415–418

Maravelaki-Kalaitzaki P, Bakolas A, Moropoulou A (2003) Physico-chemical study of Cretan ancient mortars. Cem Concr Res 33(5): 651–661

Melis S, Columbu S (2000) Matériaux de construction en époque romaine et aves les anciennes carrières: l'exemple du théâtre de Nora (Sardaigne SO, Italie). In: Lorenz J, Tardy D, Coulon G, Proceedings of La pierre dans la ville antique et médiévale. Analyse méthodologie et apports, Argentoun sur Creuse, France, 29–31 March 1998. Saint-Marcel, Musée d'Argentomagus (Ed.), pp. 103–117

Miriello D, Barca D, Bloise A, Ciarallo A, Crisci GM, Rose TD, Gattuso C, Gazineo F, Russa MFL (2010) Characterisation of archaeological mortars from Pompeii (Campania, Italy) and identification of construction phases by compositional data analysis. Journal of Archaeological Science 37(9):2207–2223

Miriello D, Barca D, Bloise A, Ciarallo A, Crisci GM, De Rose T, Gattuso C, Gazineo F, La Russa F (2010a) Characterisation of archaeological mortars from Pompeii (Campania, Italy) and identification of construction phases by compositional data analysis. J Archaeol Sci 37:2207–2223

Miriello D, Bloise A, Crisci GM, Barrese E, Apollaro C (2010b) Effects of milling: a possible factor influencing the durability of historical mortars. Archaeometry 52(4):668–679

Miriello D, Bloise A, Crisci GM, Apollaro C, La Marca A (2011) Characterization of archeological mortars and plasters from Kyme (Turkey). Journal of archeological science 38:794–804

Miriello D, Antonelli F, Apollaro C, Bloise A, Bruno N, Catalano E, Columbu S, Crisci GM, De Luca R, Lezzerini M, Mancuso S, La Marca A (2015) New data about the ancient mortars from the archaeological site of Kyme (Turkey): compositional characterization. Per Mineral 84:497–517

Morbidelli L (2003) In: Le rocce e i loro costituenti. Bardi Editore, Roma

Moropoulou A, Bakolas A, Bisbikou K (1995) Characterization of ancient, byzantine and later historic mortars by thermal and x-ray diffraction techniques. Termochimica Acta 269-270:779–795

Moropoulou A, Bakolas A, Bisbikou K (1999) Investigation of the technology of historic mortars. J Cult Herit 1:45–58

Moropoulou A, Bakolas A, Bisbikou K (2000) Investigation of the technology of historic mortars. J Cult Herit 1:45–58

Moropoulou A, Cakmak AS, Biscontin G, Bakolas A, Zendri E (2002) Advanced Byzantine cement based composites resisting earthquake stresses: the crushed brick/lime mortars of Justinian's Hagia Sophia. Constr Build Mater 16:543–552

Moropoulou A, Bakolas A, Aggelakopoulou E (2003a) Evaluation of pozzolanic activity of natural and artificial pozzolans by thermal analysis. Thermochim Acta 420:135–140

Moropoulou A, Polikreti K, Bakolas A, Michailidis P (2003b) Correlation of physicochemical and mechanical properties oh historical mortars and classification by multivariate statistics. Cem Concr Res 33:891–898

Moropoulou A, Bakolas A, Aggelakopoulou E (2004) Evaluation of pozzolanic activity of natural and artificial pozzolans by thermal analysis. Thermochim Acta 420:135–140

Moropoulou A, Bakolas A, Anagnostopoulou S (2005) Composite materials in ancient structures. Cem Concr Compos 27:295–300

Moropoulou A, Bakolas A, Moundoulas P, Aggelakopoulou E, Anagnostopoulou S (2013) Optimization of compatible restoration mortars for the earthquake protection of Hagia Sophia. J Cult Herit 14S:147–152

Ortega LA, Zuluaga MC, Olazabal A (2008) Geochemical characterization of archaeological lime mortars: Provenance inputs. Archaeometry 50(3):387–408

Paama L, Pitkänen I, Rönkkömäki H, Perämäki P (1998) Thermal and infrared spectroscopic characterization of historical mortars. Thermochimica Acta 320 (1-2):127–133

Palmstrom A (1995) RMi-a rock mass characterization system for rock engineering purposes. Ph.D. thesis. University of Oslo, Norway

Palomo A, Blanco Varela MT, Martinez Ramirez S, Puertas F, Fortes C (2002) Historic mortars: characterization and durability: new tendencies for research. Madrid: Eduardo Torroja Institute (CSIC)

Palomo A, Blanco-Varela MT, Martinez-Ramirez S, Puertas F, Fortes C (2011) Historic mortars: characterization and durability. New tendencies for research. Eduardo Torroja Institute, Madrid

Papayianni I, Pachta V, Stefanidou M (2013) Analysis of ancient mortars and design of compatible repair mortars: the case study of Odeion of the archaeological site of Dion. Constr Build Mater 40:84–92

Peccerillo A (2005) Plio-Quaternary volcanism in Italy. Petrology, geochemistry, geodynamics. Springer, Heidelberg

Pensabene P, Antonelli F, Lazzarini L, Cancelliere S (2012) Provenance of marble sculptures and artifacts from the so-called Canopus and other buildings of "Villa Adriana" (Hadrian's Villa, Tivoli, Italy. Journal of Archaeological Sciences 39:1331–1337

Pollione MV (15 BC) De Architecture. Vol. II. In: Cesariano C, De Architectura Libri Dece, 1521, Como

Riccardi MP, Duminuco P, Tomasi C, Ferloni P (1998) Thermal, microscopic and x-ray diffraction studies on some ancient mortars. Thermochim Acta 321(1-2):207–214

Salza Prina Ricotti M (2000) Villa Adriana il sogno di un imperatore: Architettura, arte e giardini. L'Erma di Bretschneider, Roma

Smith P, Smith RM (2009) Bricks and mortar: a method for identifying construction phases in multistage structures. Hist Archaeol 43:40–60

Stanislao C, Rispoli C, Vola G, Cappelletti P, Morra V, De Gennaro M (2011) Contribution to the knowledge of ancient Roman seawater concretes: Phlegrean pozzolan adopted in the construction of the harbour at Soli-Pompeiopolis (Mersin, Turkey). Periodico di Mineralogia 80(3):471–488

Topçu IB, Isıkdag B (2013) The effect of ground granulated blast-furnace slag on properties of Horasan mortar Burak Ißsıkdag. Constr Build Mater 40:448–454

Verdiani G, Columbu S (2010) E. Stone, an archive for the Sardinia monumental witnesses. Third International Conference, EuroMed 2010, Lemessos, Cyprus, November 8–13, 2010. Book Chapter. 'Lecture Notes in Computer Science' (LNCS), Springer. Berlin-Heidelberg 6436:356–372

Verdiani G, Columbu S (2012) E.Stone, an archive for the Sardinia monumental witnesses. International Journal of Heritage in the Digital Era 1(1):75–102

Verduchi P (1975) Le Terme con cosiddetto Heliocaminus a Villa Adriana. Quaderni dell'Istituto di Topografia Antica 8:55–95

Vola G, Gotti E, Brandon C, Oleson JP, Hohlfelder RL (2011) Chemical, mineralogical and petrographic characterization of Roman ancient hydraulic concretes cores from Santa Liberata, Italy, and Caesarea Palestinae, Israel. Periodico di mineralogia 80(2):317–338

Wentworth CK (1922) A scale of grade and class terms for clastic sediments. J Geology 30:377–392